M. AL-TEMEMY

ATILIM UNIVERSITY

DEVELOPMENT OF HIGH PERFORMANCE BIMETALLIC CATALYSTS FOR PROTON EXCHANGE MEMBRANE FUEL CELL

MOGDAM GASSY HUSSEIN AL-TEMEMY

January 2020

DEVELOPMENT OF HIGH PERFORMANCE BIMETALLIC CATALYSTS FOR PROTON EXCHANGE MEMBRANE FUEL CELL

A THESIS SUBMITTED TO

THE GRADUATE SCHOOL OF NATURAL AND APPLIED SCIENCES

OF

ATILIM UNIVERSITY

BY

MOGDAM GASSY HUSSEIN AL-TEMEMY

IN PARTIAL FULFILLMENT OF THE REQUIREMENTS

FOR

THE DEGREE OF MASTER OF SCIENCE

IN

THE DEPARTMENT OF CHEMICAL ENGINEERING AND APPLIED CHEMISTRY

January 2020

Approval of the Graduate School of Natural and Applied Sciences, Atılım University.

_____

Prof. Dr. Ali KARA
Director

I certify that this thesis satisfies all the requirements as a thesis for the degree of Master of Science in Chemical Engineering and Applied Chemistry, Atılım University.

_____

Prof. Dr. Şeniz ÖZALP YAMAN
Head of Department

This is to certify that we have read the thesis DEVELOPMENT OF HIGH PERFORMANCE BIMETALLIC CATALYSTS FOR PROTON EXCHANGE MEMBRANE FUEL CELL submitted by Mogdam Gassy Hussein Al-Tememy and that in our opinion it is fully adequate, in scope and quality, as a thesis for the degree of Master of Science.

_____

Assoc. Prof. Dr. Yılser DEVRİM
Supervisor

Examining Committee Members:

Prof. Dr. Necati ÖZKAN
Polymer Science and Engineering Dept,
Middle East Technical University _____

Assoc. Prof. Dr. Yılser DEVRİM
Energy Systems Engineering Dept. Atılım University _____

Assit. Prof. Dr. Enver GÜLER
Chemical Engineering and Applied Chemistry Dept. _____
Atılım University

Date: *23.01.2020*

I hereby declare that all information in this document has been obtained and presented in accordance with academic rules and ethical conduct. I also declare that, as required by these rules and conduct, I have fully cited and referenced all materials and results that are not original to this work.

Name, Last Name: Mogdam Gassy Hussein AL-Tememy

Signature:

ABSTRACT

DEVELOPMENT OF HIGH PERFORMANCE BIMETALLIC CATALYSTS FOR PROTON EXCHANGE MEMBRANE FUEL CELL

AL-Tememy, Mogdam Gassy Hussein
M.S., Chemical Engineering and Applied Chemistry
Supervisor: Assoc. Prof. Dr. Yılser Devrim

January 2020, 76 pages

Despite the growing energy demand due to the growing population and lack of fossil fuels, which is a serious concern, there must be an alternative source where research focused on renewable energy sources. Proton Exchange Membrane Fuel Cell (PEMFC) is an important and alternative technology worldwide in automotive, portable and stationary applications due to their high-efficiency, zero-emission, lightweight, fast start-up and shut down properties. High Temperature PEMFC (HT-PEMFC) eliminates some of the issues facing Low Temperature PEMFC (LT-PEMFC) such as carbon monoxide (CO) poisoning, humidity, heat and water management.

In this thesis, Multiwalled Carbon Nanotube Doped Graphene Nanoplatelet (MWCNT-GNP), MWCNT and GNP have been used as catalyst supports for the Pt:Pd bimetallic catalysts of the HT-PEMFC. The study of the dispersion of the catalyst nanoparticles on the different supports was achieved by using microwave assisted synthesis. The morphology, chemical structure and the percentage metal ratio of catalysts were characterized by using X-ray diffraction (XRD), Thermogravimetric Analysis (TGA), Transmission Electron Microscopy (TEM) and Inductively Coupled Plasma-Mass Spectroscopy (ICP-MS). TGA has confirmed the improved thermal stability of catalysts.

TEM was demonstrated dispersion and uniform distribution of the catalysts. The Electrochemical Surface Area (ECSA) of the catalysts was determined by using Cyclic Voltammetry (CV) method. ECSA of Pt:Pd/MWCNT-GNP catalyst and Pt:Pd/GNP and Pt:Pd/MWCNT catalysts were calculated as 43.8 m^2/g, 53.5 m^2/g and 71.7 m^2/g, respectively. The lowest ECSA loss was determined at 48 % in Pt:Pd/MWCNT-GNP catalyst. The results indicated that better deposition, uniform distribution and higher electrochemical surface area of the Pt:Pd/MWCNT-GNP catalyst compared to the other catalysts. The performance of the bimetallic catalyst has been confirmed on the HT-PEMFC performance test based with the pure H_2/air and reformate gas/air experiment at 160°C. Results of experimental performance test showed the current density at 0.6 V is 0.3 A/cm^2 and 0.24 A/cm^2 with pure H_2/air and reformate gas/air, respectively for Pt:Pd/MWCNT-GNP catalyst. If HT-PEMFC performance results are compared, it is determined that the best performing catalyst is Pt:Pd/MWCNT-GNP catalyst.

Keywords: Bimetallic catalyst, MWCNT-GNP Hybrid, High temperature proton exchange membrane fuel cell, microwave assisted synthesis, cyclic voltammetry.

ÖZ

PROTON DEĞİŞİM MEMBRANLI YAKIT HÜCRESİ İÇİN YÜKSEK PERFORMANSLI BİMETALLİK KATALİZÖR GELİŞTİRİLMESİ

AL-Tememy, Mogdam Gassy Hussein
Yüksek Lisans, Kimya Mühendisliği ve Uygulamalı Kimya
Tez Yöneticisi: Doç. Dr. Yılser Devrim

Ocak 2020, 76 Sayfa

Artan nüfus ve azalan fosil yakıtlar nedeniyle ciddi bir endişe kaynağı olan enerji ihtiyacındaki artış araştırmacıları alternatif bir kaynak olarak yenilenebilir enerji kaynaklarına yönlendirmiştir. Proton Değişim Membranlı Yakıt Hücresi (PEMFC) yüksek verimliliği, hafif olması, düşük emisyon, hızlı başlatma ve kapatma gibi özellikleri nedeniyle taşınabilir ve sabit uygulamalarda dünya çapında önemli ve alternatif bir teknolojidir. Yüksek sıcaklık PEMFC (HT-PEMFC), düşük sıcaklık PEMFCde (LT-PEMFC) yaşanan karbon monoksit (CO) zehirlenmesi, nemlendirme, ısı ve su yönetimi sorunlarını azalttığı için tercih edilmektedir.

Bu tezde, HT-PEMFC için sentezlenen Pt:Pd bimetalik katalizörlerinin hazırlanmasında katalizör desteği olarak çok duvarlı karbon nanotüp yüklenmiş grafen nanoplaka (MWCNT-GNP), MWCNT ve GNP kullanılmıştır. Katalizör metallerin farklı desteklere dağılımı, mikrodalga yöntemi kullanılarak gerçekleştirilmiştir. Katalizörlerin metallerinin morfolojisi, kimyasal yapısı ve yüzde oranı, X-ışını kırınımı (XRD), termal gravimetrik analiz (TGA), transmisyon elektron mikroskobu (TEM) ve indüktif olarak eşleşmiş plazma kütle spektroskopisi (ICP-MS) kullanılarak tanımlanmıştır. TGA analizi katalizörlerin termal kararlılığının arttığı doğrulanmıştır. TEM ile dispersiyon ve katalizörlerin

düzgün ve homojen dağılımı gösterilmiştir. Katalizörlerin elektrokimyasal yüzey alanı (ECSA), döngüsel voltametri (CV) yardımı ile hesaplanmıştır. Pt:Pd/MWCNT-GNP, Pt:Pd/GNP ve Pt:Pd/MWCNT katalizörleri için ECSA sırası ile 43.8 m^2/g, 53.5 m^2/g ve 71.7 m^2/g'dır. En düşük ECSA kaybı % 48 olarak PtPd/MWCNT-GNP katalizöründe elde edilmiştir. Sonuçlar, Pt:Pd/MWCNT-GNP'nin daha iyi birikim, homojen dağılım ve diğer katalizörlere kıyasla daha yüksek ECSA sayesinde HT-PEMFC için daha uygun bir katalizör olduğunu göstermiştir. Bimetalik katalizörlerin performansı, bu MEA'ler ile hazırlanan tek hücreli HT-PEMFC'e 160 ^oC'de saf H_2, reformat gaz ve kuru hava beslemelerinde test edilmiştir. Sonuçlar içerisinde en iyi sonuçları Pt-Pd/MWCNT-GNP katalizörü, 0.6 V'da saf H_2/hava ve reformat gaz/hava beslemeleri için sırasıyla 0.3 A/cm^2 ve 0.24 A/cm^2 akım yoğunlukları ile göstermişlerdir.

Anahtar Kelimeler: Bimetalik katalizör, MWCNT-GNP, Yüksek Sıcaklık Proton Değişim Membranlı Yakıt Hücresi, Mikrodalga Sentez Yöntemi, Döngüsel Voltammetri

To My Family

ACKNOWLEDGMENTS

I would like to express my sincere thanks and gratitude to supervisor Assoc. Prof. Dr. Yılser Devrim for her guidance, criticism, encouragement, insight, invaluable and indisputable advice, and patience throughout the research period. The biggest thanks to her for teaching me about fuel cells that could give me the opportunity to work and experience in the future.

I shall also thank to the lab colleague, PhD student Yağmur Budak for her kind help and cooperation as well as for her support in preparing the catalysts in the lab and my other colleague Yağmur Özdemir for preparing PBI polymers.

Furthermore, thank you to my deceased father, my mother, my family for their patience and support for me, and everyone who gave me a hand and help from my loved ones and friends.

TABLE OF CONTENTS

LIST OF TABLES

LIST OF FIGURES

LIST OF SYMBOLS/ABBREVIATIONS

AFC	Alkaline Fuel Cell
Ag	Silver
AgCl	Silver Chloride
BL	Backing Layer
BPP	Bipolar Plates
CB	Carbon Black
CC	Carbon Cloth
CCM	Catalyst Coated Membrane
CE	Counter Electrode
CFP	Carbon Fiber Paper
CHP	Combine Heat and Power
CL	Catalyst Layer
CNT	Carbon Nanotube
CO	Carbon Monoxide
CO_2	Carbon Dioxide
CO_3^{-2}	Carbonate
CTAB	Cationic Cetyltrimethylammonium Bromide
CV	Cyclic Voltammetry
DI	Deionized Water
DL	Diffusion Layer
DMAc	N-N dimethylacetamide
DMFC	Direct Methanol Fuel Cell
E	Potential (Volt)
ECSA	Electrochemical Surface Areas
EG	Ethylene Glycol
EPDM	Ethylene-Propylene-Diene-Monomer
F	Faraday Constant (A.s/mole)
FC	Fuel Cell
FCC	Face-Centered Cubic
FWHM	Full Width Half Maximum

GC	Glassy Carbon
GDE	Gas Diffusion Electrode
GDL	Gas Diffusion Layer
G-MWCNT	Graphene-Multiwall Carbon Nanotube
GNP	Graphene Nanoplatelet
H_2	Hydrogen
H_2O	Water
$H_2PtCl_6.6H_2O$	Hexachloroplatinic Acid Hexahydrate
H_2SO_4	Sulfuric Acid
H_3PO_4	Phosphoric Acid
HCL	Hydrochloric Acid
HER	Hydrogen Evolution Reaction
hf	Heat Formation of Reactants and Products
HOR	Hydrogen Oxidation Reaction
HT-PEMFC	High Temperature PEMFC
$HClO_4$	Perchloric Acid
HNO_3	Nitric Acid
ICP-MS	Inductively Coupled Plasma-Mass Spectroscopy
IPA	Isopropyl Alcohol
IRR	Butyl Rubber
K	Potassium
K_2PtCl_6	Potassium Hexachloroplatinate (IV)
KOH	Potassium Hydroxide
Li	Lithium
$LiAlO_2$	Lithium Aluminum Oxide
LT-PEMFC	Low Temperature PEMFC
$m_{(PtPd)}$	The Weight of PtPd Catalyst
MCFC	Molten Carbonate Cell Fuel
MEA	Membrane Electrode Assembly
MFC	Mass Flow Controller
MPL	Microporous layer
MWCNT	Multiwall Carbon Nanotube
n	Number of Electrons Transferred

NaCl	Sodium Chloride
NaOH	Sodium Hydroxide
Ni	Nickel
NPG	Nitrogen-rich Graphene Nanopores
N_2 rich G	Nitrogen Rich Graphene
N_2_MWCNT	Nitrogen Doped MWCNT
N_{Avg}	The Avogadro Number (6.02 x 1023)
O_2	Oxygen
OCV	Open Circuit Voltage
OH^-	Hydroxide
ORR	Oxygen Reduction Reaction
PA doped PBI	Phosphoric Acid Doped Polybenzimidazole
PAFC	Phosphoric Acid Fuel Cell
PBI	Polybenzimidazole
$Pd(acac)_2$	Palladium(II) bis(acetylacetonate)
$PdCl_2$	Palladium(II) Chloride
PDMS	Polydimethylsiloxane
PdPc	Palladium Phthalocyanine
PEMFC	Proton Exchange Membrane Fuel Cell
PFSA	Perfluorosulfonic acid
PI	Pressure Indicator
PIC	Pressure Indicator and Controller
ppm	Parts Per Million
PR	Pressure Regulator for Hydrogen
Pt	Platinum
$Pt(acac)_2$	Platinum(II) bis(acetylacetonate)
PTFE	Polytetrafluoroethylene
PtPc	Platinum Phthalocyanine
PVDF	Polyvinylidene Difluoride
q	The Charge (Coulombs mol^{-1})
RDE	Rotating Disk Electrode
RE	Reference Electrode
RH	Relative Humidity

rpm	Revolutions Per Minute
Rs	Raman Spectroscopy
SAED	Selected Area Electronic Diffraction
$scCO_2$	Supercritical Carbon Dioxide Method
SDS	Anionic Sodium Dodecyl Sulfate
SEM	Scanning Electron Microscopy
sf	The Entropy of Products and Reactants
SOFC	Solid Oxide Fuel Cell
SPE	Solid Polymer Electrolyte
SSA	Specific Surface Area (m^2/g)
STEM	Scanning Transmission Electron Microscopy
SV	Selenoid Valve
SV2	Purge Selenoid Valve
SWCNT	Single wall Carbon Nanotube
T	Temperature (K)
TEM	Transmission Electron Microscopy
Tg	Glass Transition Temperature
TGA	Thermogravimetric Analysis
TIC	Temperature Indicator and Controller
TPB	Three-Phase Boundary
U_{PtPd}	Utilization Efficiency (%)
W	The Electrical Work ($J\ mol^{-1}$)
WE	Working Electrode
XPS	X-ray Photoelectron Spectroscopy
XRD	X-ray Diffraction
ZrO_2	Zirconium Oxide
H^+	Hydrogen ion
q_{el}	The Charge of an Electron (Columbus/electron)
E_a^0	Potential of Anode
E_c^0	Potential of Cathode
Q_H	The Charge of Hydrogen Adsorption/Desorption
ΔG	Gibbs Free Energy
ΔH	Enthalpy of the Chemical Reaction

ΔS	The Entropy Change of the Reaction
2D	Two-Dimensional
η	Efficiency
$\boldsymbol{\theta}$	The Angle at The Maximum of the Peak
ρ	The density of Pt metal
$\boldsymbol{\lambda}$	Wavelength of X-ray diffraction

CHAPTER 1

1. INTRODUCTION

1.1. Fuel Cell (FC)

Due to the increasing population, the need for fossil fuel consumption is increasing, as it meets nearly 80 % of the world's energy. The result of the petroleum company assessment, the highest levels of production of fossil fuels, oil, and natural gas will be between 2015-2020 and then begins to decline and depletion in the future in addition to causing many environmental problems such as climate change, rising sea levels, acid rain, pollution, ozone layer depletion, forest and agricultural land damage caused by surface mining of coal where these problems cost about $5 trillion per year [1].

In the 21st century, there are great challenges for the development and storage of clean energy sources. Many efforts and research on improving the performance of FC technologies from these sources at lower cost have attracted great attention [2]. FC is a device that converts the chemical energy of Hydrogen (H_2) and Oxygen (O_2) directly into electrical energy, water, and heat by the presence of the catalyst as shown in Figure 1.1. [3].

The FC and batteries are similar in structure and operating principles. Both converts chemical energy into electricity, as well as FC containing two electrodes and electrolyte. On the other hand, the batteries are a source of independent or portable electricity, containing chemical substances, which cannot save energy after it is exhausted. Batteries are in various forms and their reactions use diverse chemical substances to produce electricity. While the FC does not contain chemical substances, so it is supplied from an external source and thus generates continuous energy.

FCs are unique because of the operation reactions. In the FC, reacting gases are not mixed. H_2 is supplied with one of the electrodes called the anode while the O_2 is supplied to the other electrode which is called the cathode. An electrolyte is used to separate the two electrodes from each other. The electrolyte is the fundamental part of an electrochemical cell because it prevents the mixing of reactant materials with each other, prevents the passage of electrons, while allows the passage of protons, non-permeable gases, H_2 and O_2. H_2 and O_2 ions combine to produce water. The electron passes from the anode to the cathode via an external circuit where it does not pass through the electrolyte.

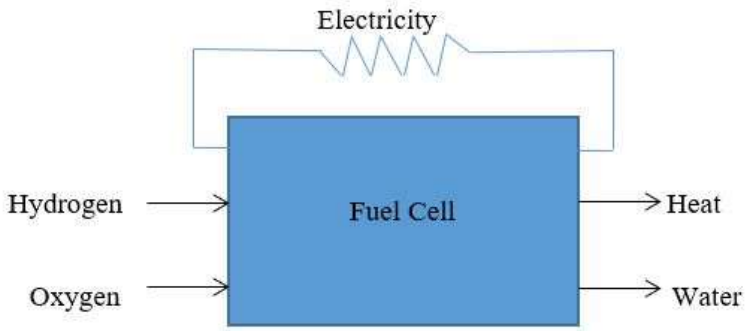

Figure 1.1. A simple diagram of FC

Conventional technology has more steps for electric production than FC and the efficiency less than 30 %, while the efficiency of the FC is about 50 % in one step. Theoretically, the maximum efficiency of the H_2 FC at room temperature is up to 83% [4], [5].

FC are a promising candidate for future energy sources because they have several advantages such as zero-emission, high efficiency, noise-free, no moving parts, modularity, and simplicity compared to conventional energy technologies. FC have begun to put their mark on the commercial markets and produce profits for some companies [6], [3].

1.2. History of FC

The process of electrolysis of the chemical interaction between O_2 and H_2 was demonstrated by Sir William Grove in 1839, where the two electrodes are placed in the water and the H_2 reaction on one electrode and then O_2 on the other is the fundamental of the FC work [5].

The first FC was designed by scientist Grove during that period. The device was called a “gaseous voltaic battery”, consisting of two electrodes of Platinum (Pt) immersed in the sulfuric acid. One of the electrodes contains the O_2 and the other electrode contains H_2 [7]. One of Grove's limitations is the lack of current generated.

In 1889, Charles Langer and Ludwing Mond modified the Grove device and was later renamed the device as a FC. In 1893, Friedrich W. Ostwald found there a relationship between the main components of FC, such as electrodes and electrolytes.

The first alkaline FC (AFC) was described by an English engineer, Francis T. Bacon in 1932, after this time also was developed a 6 kW FC stack at the end of the 1950s. In 1942, W. F. Ostwald explained how FC work [1], [8], [7].

The Molten Carbonate FC (MCFC) was announced by Dutch scientists Broes and Ketelaar in the 1950s [7]. The first FC was used in the US space program. The first Proton Exchange Membrane FC (PEMFC) was investigated by the General Electric company in the early 1960s where it was employed in the US Gemini program [8].

In1960s, Nafion membrane showed good durability and performance in the use of applications. In 1973, many governments motivations the use of FC as an alternative source of the oil crisis in electricity generation [7]. Environmental impacts were observed in 1980 and as a result of emissions of gasoline-powered vehicles, PEMFC technology is one of the technologies that reduce environmental impacts. Other types of FC have been developed, especially those operating at high temperatures such as the MCFC and the SOFC [5]. At the beginning of the twentieth century, the SOFC was created [7]. In 1986, D.S Watkins developed the experimental membrane of PEMFC [8]. In 1992, International FC showed the first commercial FC energy generation based on acid electrolyte, the Phosphoric Acid FC (PAFC) [5]. FC buses described by Ballard Power Systems where the first PEMFC car was evinced in 1993 [1]. Start commercialization of FC from the beginning of 2000 for use in transportation applications, trade and industrial power generation [7]. Figure 1.2 illustrates a diagram for the development of FC history.

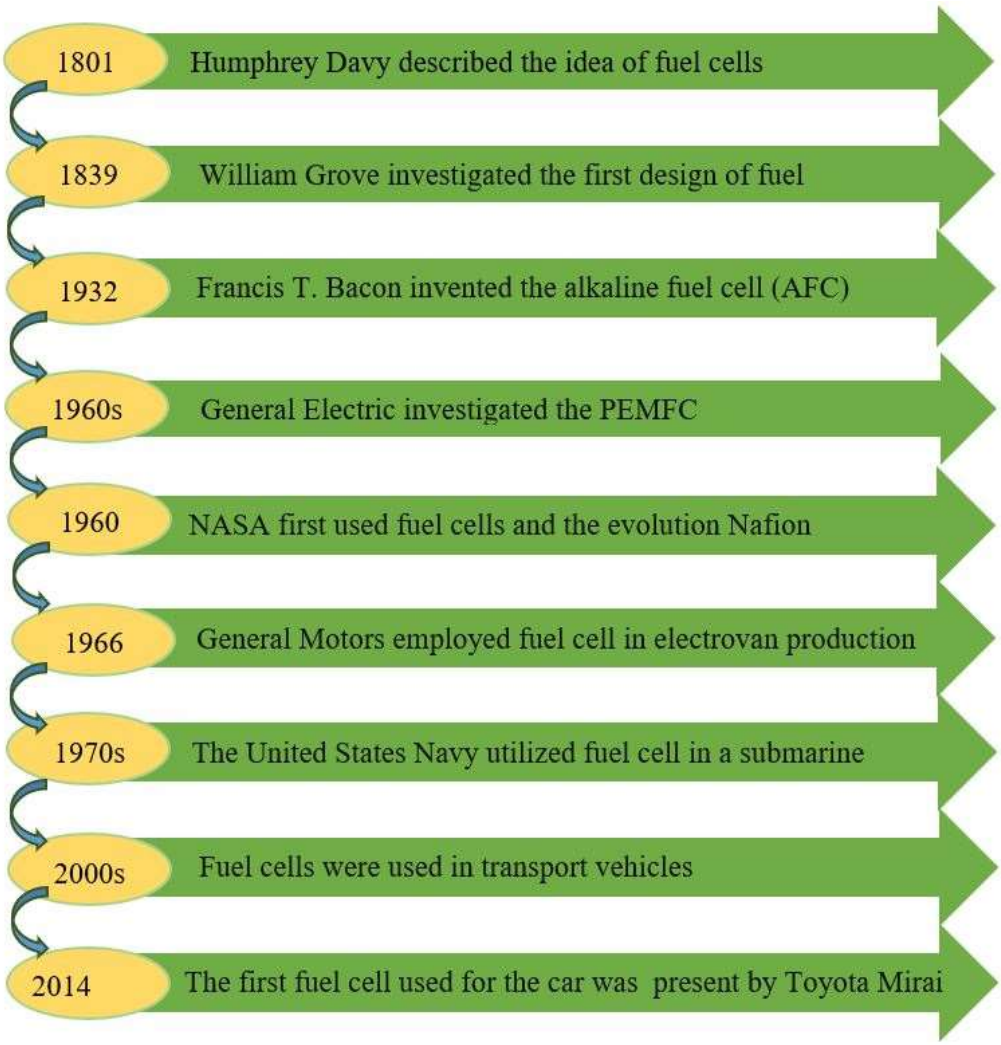

Figure 1.2. History of FC development [7], [1]

1.3. Types of the FC

FC are classified into several types where their name depends on the type of electrolyte used for each of them, as shown in Table 1.1.

Table 1.1. FC Types [9], [1], [5]

Fuel Cell Types	Mobile Ion	Temperature (°C)	Electrical Efficiency(%)	Power (kW)	Applications
AFC	OH^-	150-200	62	10-200	Space stations
PAFC	H^+	150-200	40	< 10,000	Hydrogen production
MCFC	CO_3^{-2}	650	47	< 100,000	High power plants
SOFC	H^+or O^{-2}	1000	55 – 60	< 100,000	High power plants
PEMFC	H^+	80-200	30 – 50	0.002-500	Transportation industries
DMFC	H^+	30-80	25 – 40	< 0.2	Hydrogen production

1.3.1. Alkaline Fuel Cell (AFC)

Potassium hydroxide (KOH) is used as an electrolyte which can operate high temperatures such as 250°C with a higher concentration ratio. Also, this type of electrolyte can operate low temperatures such as 120°C with a lower concentration ratio. Large-scale electrocatalysts such as Nickel (Ni), silver (Ag), metal oxides, and noble metals are used. H_2 is provided at the anode where it is divided into H_2 atoms containing electrons and protons. The O_2 molecules are separated to form atoms at the cathode side. This type has been used in the space program (Apollo and Space Shuttle) since the 1960s and this is non-tolerant of CO_2. AFC has an efficiency of approximately 60 %. The cell life of the space shuttle is about 2,600 hours. Modern development is looking for the arrival of cell life to 5,000 hours [1], [5], [10]. But one of the constraints facing AFC is the sensitivity of the hydroxide electrolyte to the carbonatation, where carbonates formation inside the alkaline electrolyte, resulting in the production of solid carbonate crystals that impede the electrolyte and inhibit the spread of gases to the active catalyst layers (CL) and disturb the mechanical stability [11].

1.3.2. Phosphoric Acid Fuel Cell (PAFC)

PAFC growth has happened in the United States and Japan, the first commercial unit launched in 1992 by a US company. PAFC uses pure phosphoric acid (H_3PO_4) as an electrolyte. The electrode layer is made of carbon paper. PAFC uses Pt or alloys as a catalyst. This type of FC operates temperatures between 150-200°C with H_2 and O_2 gases. FC efficiency typically ranges from 36 % to 42 % and the efficiency increased with increasing pressure. PAFC possesses several unique features such as high stability in corrosion environment, high resistance to pollutants and good ionic conductivity. The cell life is up to 40,000 hours, which gives it good quality for operation [5], [12].

1.3.3. Molten Carbonate Fuel Cell (MCFC)

The work of this type of FC was begun in the 1950s after the period of research was presented in the 1930s. The operating temperatures of MCFC are higher than 660°C, therefore do not require noble metal catalysts. MCFC uses electrolyte made of a lithium–potassium (Li-K) at atmospheric pressure or Na-Ni at a higher pressure than atmospheric able of carrying an alkaline carbonate mixture retrained in a porous aluminate matrix of lithium aluminum oxide ($LiAlO_2$). The MCFC is deemed more complex and cost-effective than other types of FC. The reaction of MCFC consists of H_2 at the anode and carbon dioxide (CO_2), where react with O_2 at the cathode in order to generate carbonate ions in the electrolyte then react with H_2. The efficiency of MCFC is ranging between 47-60 % and FC life is short [13], [5].

1.3.4. Solid Oxide Fuel cell (SOFC)

SOFC is considered the strongest cell types and it is unique because of the hardness of the electrolyte. SOFC use electrolyte made from zirconium oxide (ZrO_2), this also called Zirconia. This type of electrolyte for the first one time was used in the 1930s with modest success and remained in the business until the 1950s and 1960s. The reaction of SOFC consists of H_2 and O_2 as fuel and water production.

Ni is a metal used as an anode which is inefficient in the direction of H_2 while a cathode is made of conductive oxide and does not react with O_2. SOFC operating at a temperature of 1000°C with 60 % efficiency. Thanks to the high operating temperature of SOFC does not need an electric catalyst to generate O_2 and H_2 atoms.

The SOFC electrolyte hardness can give it a long lifetime, some units operate for 60,000 hours [5]. The SOFC is similar to MCFC in terms of high temperature. SOFC has the potential in applications of scale and high power rates [12].

1.3.5. Proton Exchange Membrane Fuel Cell (PEMFC)

PEMFC is divided according to the operating temperature into low-temperature (LT-PEMFC) ranging from 50-100°C, and high-temperature (HT-PEMFC) ranging from 125-200°C. PEMFC uses a thin proton conductive polymer membrane (such as perfluorosulfonic acid at low-temperature and polybenzimidazole (PBI) at high-temperature) as the electrolyte. This type of FC uses Pt or Pt-based alloy is usually used as a catalyst and carbon as support. The PEMFC are a promising candidate for automotive, stationary and portable applications. Among the various FC types, PEMFC are the most attracted by the researchers due to low reagents, high energy density, the use of solid components and low operating temperature, making them more suitable for portable applications. PEMFC has demonstrated its flexibility in a lot of various applications. The efficiency of PEMFC ranges from 30-50 %. The PEMFC lifetime of approximately 10,000 hours. Some products have a lifespan up to 40,000 hours. As a result of the development of technology and applications in our daily lives is expected to increase commercialization in the future [1], [3], [9], [14]. PEMFC has features lower sealing problems, lower operating temperature, easier scale and shorter time of start-up compared to the SOFC [15].

1.3.6. Direct Methanol Fuel Cell (DMFC)

DMFC used the same electrolyte which is used in the PEMFC. The only difference is the use of methanol liquid as anode fuel instead of H_2. The use of liquid methanol as a fuel instead of H_2 gas is more important because of its the many advantages as it reduces the cost has a high volumetric energy density and ease of transport, storage, and dealing. Pt is used as a catalyst supported on carbon. The operating temperature for DMFC is ranging between 30-90°C. According to the high current density of the DMFC, it is usually used as an alternative to Li-ion batteries in mobile devices. DMFC efficiency is estimated at 40 %, but in practice does not exceed 25 %. Cell life is also a problem because it is estimated at 1,000 hours. One of the disadvantage for DMFC is the formation of carbon monoxide (CO) due to the spread of methanol through the electrolyte from the anode to the cathode [5], [16], [17].

CHAPTER 2

2. PEMFC

At the beginning of 1960, they were known as the Solid Polymer Electrolyte FC (SPEFC). The membrane represents an electrolyte being between the porous electrodes. Between an electrolyte and the electrode is a layer with catalyst particles usually Pt supported on carbon [1]

The American General Electric Company first invented this type of cells in the early 1960s by the US military which was adopted by the US space agency NASA. In the early 1980s, it was used by the British Navy after being developed by the US Navy. The Canadian company Ballard Systems used this technology in civil transportation applications such as buses [5].

PEMFC is one of the most important and competitive techniques in place for convention energy conversion technologies and other energy sources because of its possibility of change for energy demand, zero-emission, fast start-up and shut down, lightweight, high efficiency, withstanding shocks and vibrations because of the solid material, the high intensity and simpler design and operation. Meet the requirements of stationary applications, transport and portable applications [18], [19], [20]. The improvement of PEMFC should be characterized by electrical insulation, chemically, mechanically and thermally excellent [21].

There are some barriers to marketing such as high cost, gas poisoning, loss of performance and deterioration of the membrane and durability. Another challenge facing PEMFC as acceptable to the power source is durability. PEMFC durability affected from poor water management, fuel oxidation, corrosion and chemical reaction of components [22].

The lifetime of the cells varies according to the applications, with 5,000 hours for cars up to 20,000 hours for buses and 40,000 hours for continuous operation of stationary applications. Several efforts have been devoted to the development of

PEMFC to increase their efficiency, reliability and potential power of stacks, as well as portable batteries, automotive applications and fixed residential power [23].

2.1. Operation of PEMFC

The electrochemical reactions of the PEMFC occur on the surface of the CL is given in the Figure 2.1.

H_2 is fed on one side which is negative (anode) side without any moisture and separated into two electrons and two protons at the CL[24].

Reaction at Anode:

$$H_2 \rightarrow 2H^+ + 2e^- \quad \text{(Anode, } E_a^0 = 0 \text{ V vs. SHE)} \tag{1}$$

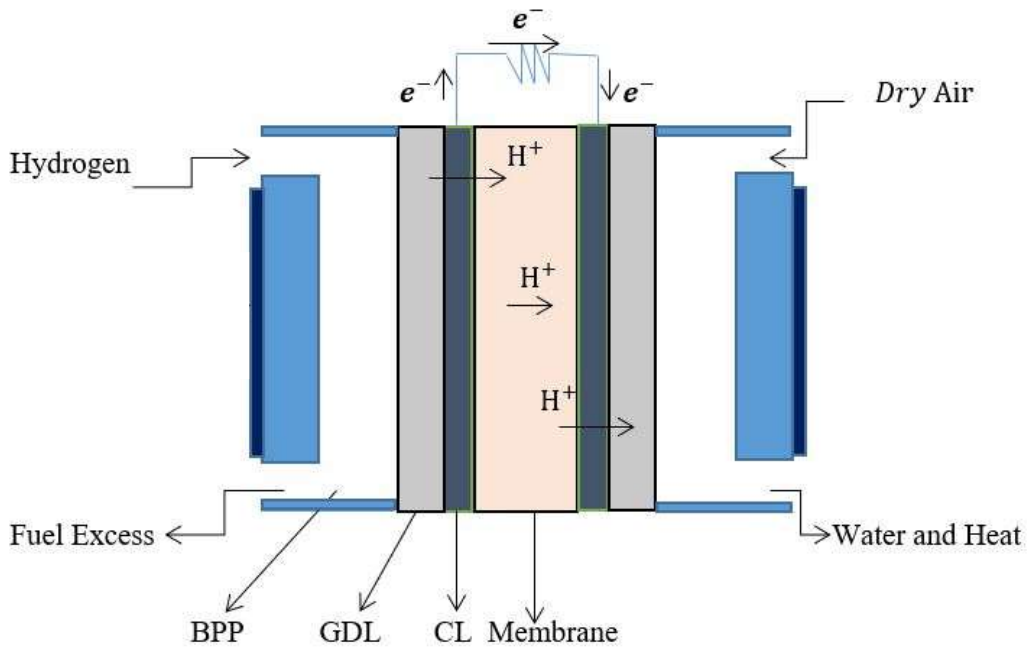

Figure 2.1. Principle operation of PEMFC

The proton moves through the membrane to the other side, while the electron moves through an external circuit. O_2 is fed on the other side which is a positive (cathode) side where the interaction occurs between proton and O_2 at the catalyst surface. The reaction product is a current and produced water is removed from the excess O_2 flow [1], [25], [26].

Reaction at Cathode:

$$\frac{1}{2}O_2 + H^+ + 2e^- \rightarrow H_2O \quad \text{(Cathode, } E_c^0 = 1.23\text{V vs. SHE)} \tag{2}$$

Overall reaction:

$$H_2 + \frac{1}{2}O_2 \rightarrow H_2O \quad (E^0\text{cell} = 1.23\text{V}) \tag{3}$$

The overall reaction is the same reaction for H_2 combustion, and it is an exothermic reaction:

$$H_2 + \frac{1}{2}O_2 \rightarrow H_2O + \text{heat} \tag{4}$$

The enthalpy is the difference between the heats of formation of products and reactants of the chemical reaction:

$$\Delta H = (hf)_{H_2O} - (hf)_{H_2} - \tfrac{1}{2}(hf)_{O_2} = -286 \text{ kJ/mol.} \tag{5}$$

At 25°C, the heat of formation of liquid water is - 286 $kJmol^{-1}$ and the heat of the formation of both H_2 and O_2 is equal to zero. Therefore, the enthalpy is equal to -286 kJ/mol. All the energy inputs and enthalpy can be converted into electricity of the reaction in a FC corresponds to Gibbs free energy and is given by the following equation:

$$\Delta G = \Delta H - T\,\Delta S \tag{6}$$

where T is the temperature in K and ΔS is the difference between entropies of products and reactants. Because of the creation of entropy, so there are some irreversible losses in the energy conversion:

$$\Delta S = (sf)_{H_2O} - (sf)_{H_2} - \tfrac{1}{2}(sf)_{O_2} \tag{7}$$

The electrical work (W) is the product of charge and potential:

$$W = q\,E \tag{8}$$

where q is charge (C mol^{-1}) and E is potential (Volts). The total charge transferred in the reaction of the FC:

$$q = n\,N_{Avg}\,q_{el} = n\,F \tag{9}$$

where, n is the number of electrons transferred for the H_2, N_{Avg} is the Avogadro number ($6.02x10^{23}$), q_{el} is the charge of an electron (1.602×10^{-9} C/electron) and F is the Faraday's constant (96485 C/mol.e^-). The electrical work is:

$$W = n F E \quad (10)$$

The maximum amount of electrical energy in the FC that generated corresponds to Gibbs free energy, ΔG:

$$W = - \Delta G \quad (11)$$

The theoretical potential value of the FC is as follows:

$$E = - \Delta G / nF \quad (12)$$

The efficiency of the energy conversion device is the ratio between the useful energy output (electrical energy produced) and energy input (enthalpy of H_2), where the theoretical efficiency of the FC is [1]:

$$\eta = \Delta G/\Delta H = 237.34/286.02 = 83\ \% \quad (13)$$

PEMFC is a promising energy conversion technology because of its high efficiency, high energy density, low CO_2 emissions and rapid start-up [27]. There are two types of PEMFCs depending on the operating temperature:

2.1.1. Low-Temperature Proton Exchange Membrane Fuel Cell

LT-PEMFC operates at temperatures between 60-80°C. LT-PEMFC is usually used perfluorosulfonic acid (PFSA) as a membrane and water is used as a proton carrier medium for LT-PEMFC [15], [23], [24].

PFSA membranes are used in LT-PEMFC to achieve good proton conductivity, high chemical stability, thermal stability, mechanical strength and elasticity. These features operate at low temperatures and high humidity because the low humidity reduces conductivity and therefore water and heat management are the important factors. Also, it has low CO tolerance at low temperatures. The PFSA membrane suffers from some issues such as water management, high hydration and low CO tolerance [28]–[30].

Water management is essential for LT-PEMFC stack design. The absence of water in the membrane causes the membrane dryness which leads to lower proton conductivity that affects the power and efficiency of the system and increased the

cell resistance. While the increase in the amount of water leads to flooding which obstructs the transfer of gases in the porous gas diffusion electrode. If the heat is low, the flood will occur, sufficient heat is essential to achieve high efficiency, high performance, and durability of the FC. The heat management system and cooling device are important for removing excess heat. An operating system for temperatures below 100°C is inefficient because it requires heat management and cooling, so the heat output is low and cannot be transferred to use in other processes. Heat rejection is more difficult when operating at low temperatures because the difference is very little or negligible between them and the surrounding environment. At the anode, the exchange current density in the H_2 oxidation reaction (HOR) is significantly higher than the exchange current intensity of the O_2 reduction reaction (ORR). This causes the slow electrochemical kinetics of the cathode, as a result of slowing the kinetics of the reaction, the excess potential at the cathode is responsible for the loss of voltage. The high working temperature heat is necessary to increase the kinetics of the reaction, but lead to the membrane dryness so water is necessary to moisten the membrane to preserve optimum performance [31]. The fuel stream must be moistened to avoid membrane dryness and thus loss of PEMFC performance, while the liquid water generated by the electrochemical reaction at the cathode causes flooding. The effect of CO in H_2 gas is absorbed on the surface of the catalyst and prevents HOR sites result in reduced catalyst activity in the anode and thus degradation of PEMFC performance. LT-PEMFCs have a lower tolerance of impurities because CO absorption on the Pt electrode increases with a lower temperature [24]. LT-PEMFC needs pure H_2 as fuel because it has little tolerance for impurities, so LT-PEMFC system is still expensive because it needs a high purity H_2 or external reactant purification systems [27]. LT-PEMFC are at the forefront of marketing as a result of rapid start-up, high energy density and high efficiency, but remain subject to several constraints such as low tolerance of impurities, complex system, low heat generation and water management difficulty (drought, flood). In order to overcome these constraints, HT-PEMFC is used [3].

2.1.2.High Temperature PEMFC

HT-PEMFC is technically more suitable than the other technologies and predicted its targets during 2020 for combined the heat and power (CHP) systems are high

electrical efficiency, excellent energy efficiency, operating life of 60,000 hours, that can be achieved by using HT-PEMFC system [3]. HT-PEMFC operates at temperatures ranging from 120-200°C [32]. The safest operation temperature of the HT-PEMFC is between 120-180°C, because the temperature below 120°C can cause water formation and temperatures higher than 180°C can cause component degradation [31]. The high operating temperatures gained considerable attention compared to the LT-PEMFC for applications of portable and stationary [33].

HT-PEMFC is an important and alternative technique for traditional LT-PEMFC because it has many advantages and characteristics as it reduces the problem of CO poisoning with high CO tolerance, facilitates water management and eliminates flooding, increases the rate of electrochemical reaction in anode and cathode that allow Pt to be replaced by economic catalyst, improves PEMFC performance, availability usage of the waste temperature with CHP systems applications which enhances the efficiency and working without wetness [24], [27], [34]–[36].

HT-PEMFC systems can be easily used inexpensive reformer systems. Thanks to the impurity tolerances of HT-PEMFC can be fed directly from a reformer system so that there is no need for a separate H_2 infrastructure and storage. The reformate gas mixture can be generated from industrial processes using natural gas or methane. Thus, the usage in the daily life of HT- PEMFC simplifies and accelerates. Generally, H_2 rich reformate gas mixture generated from the reformer contains 40-70 % H_2, 15-25 % CO_2 and 1-3 % CO [37]–[40]. The HT-PEMFC must be preferred for reformate gas applications because of their high CO tolerance [37], [38], [41].

Typically, the LT-PEMFC like the structure of the HT-PEMFC differs only by a type of membrane and some of the system components. In LT-PEMFC, the fuel must be humidified before entering the anode of FC to prevent drying of the Nafion membrane because the proton moves through the membrane where the water is used as a proton carrier. Increasing the temperature of the PEMFC lead to dry the Nafion membrane and loss of the proton conductivity, so many researchers have developed a membrane that operating at temperatures higher than 100°C and has superior advantages such as high conductivity at low humidity, in addition to low cost material and high durability [24]. As a result, the membrane used in LT-PEMFC should be replaced by a membrane that has proton conductivity which does not

depend on the water at high temperatures. One of the membrane types used for this purpose is a H_3PO_4 doped PBI, it has excellent chemical stability, mechanical strength, low cost, thermal stability, durability and proton conductivity under anhydrous condition [3], [33], [42]. For HT-PEMFC, H_3PO_4 is used as a carrier medium for proton like water which used in LT-PEMFC.

The transfer resistance of a proton and charger decreases with increasing temperature and thus, increases the effectiveness of the kinetics of an electrochemical reaction due to reduced membrane resistance. By increasing the temperature of the fuel, where the concentration of O_2 and water in the cathode hardly changes as evidence that the increasing temperature not only enhances the rate of an electrochemical reaction but improves the transfer of O_2 and water in the cathode, thus compensating O_2 consumption and water production in the CL as well as increased current density and thus the ORR increased [31], [43].

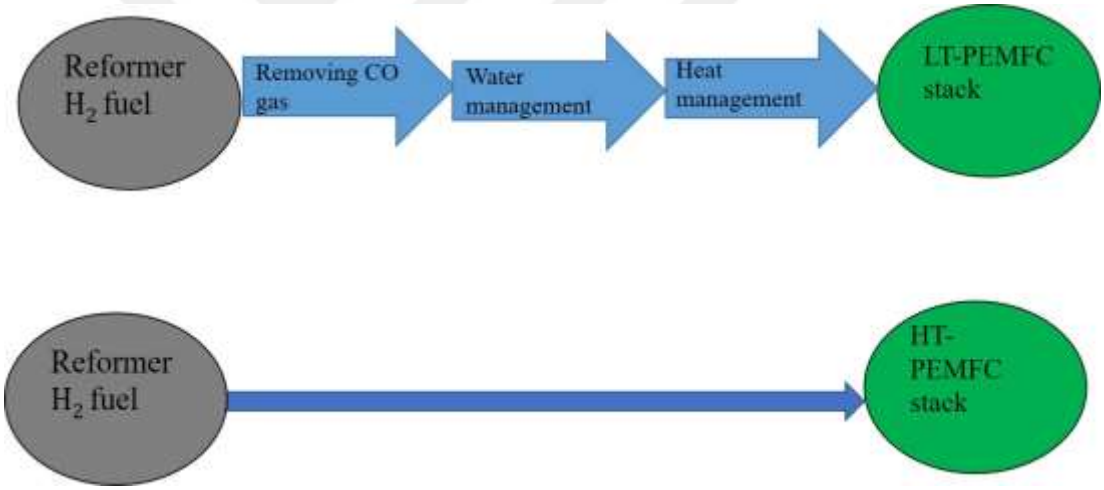

Figure 2.2. Diagram of different HT-PEMFC and LT-PEMFC

Cooling systems ensure homogeneous temperature by removing excess temperature in PEMFC stack and cells. Therefore; the cooling system is important for both HT-PEMFC and LT-PEMFC systems because of the electrochemical reaction generates heat as a byproduct [31]. The cost of power generation can be reduced using HT-PEMFC excess heat in the reformate system. The advantages of HT-PEMFC superior on LT-PEMFC shown in Figure 2.2 and also summarized in the Table 2.1 [36].

Table 2.1. Comparison between LT-PEMFC and HT-PEMFC

Name of items	LT-PEMFC	HT-PEMFC
Membrane	Perfluoro-sulfonic acid	Polybenzimidazole
Electrode	Carbon support Pt or Pt alloys catalyst	Carbon support Pt or Pt alloys catalyst
Operating temperature	70 – 80°C	120 – 180°C
Efficiency	40 %	45 – 50 %
Proton transport media	Water	Inorganic acid
CO tolerance	< 50 ppm	1 - 3 % by volume
Water and heat management	Complex	None
Reaction rate	Low	High

2.2. Main components of HT-PEMFC

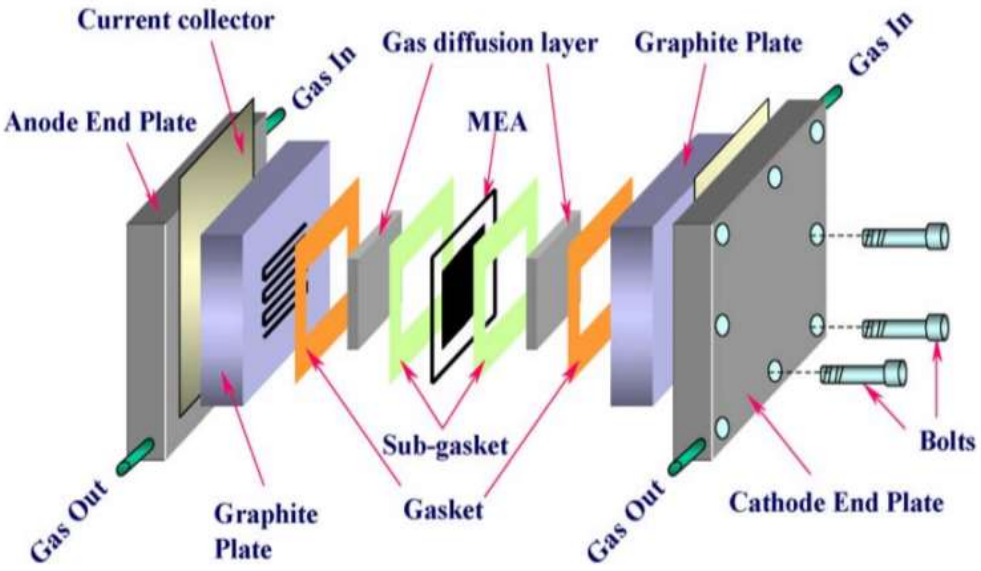

Figure 2.3. The main component of PEMFC

A single HT-PEMFC consists of one proton exchange membrane, two CL, two gas diffusion layers (GDL), two gaskets, two bipolar plates (BPP), two current collector

and two end plates[44]. Figure 2.3 illustrates the main components of HT-PEMFC [45].

2.2.1. Membrane

Membrane, which is made from polymer, is the heart of the cell. The membrane where represents the electrolyte that is located between two porous electrodes running of proton transport, supporting both anode and cathode CL [1]. The membrane thickness typically ranges from 50 to 175 μm which is equivalent to seven sheets of paper [5]. PFSA membrane such as the Nafion commonly used in LT-PEMFC due to high chemical stability, excellent mechanical properties and high proton conductivity at 80°C and surrounding pressure [6],[36],[46],. Figure 2.4 illustrates the chemical structure of PFSA where x=2,4 or 7; y=1; m=1; n=2 [47].

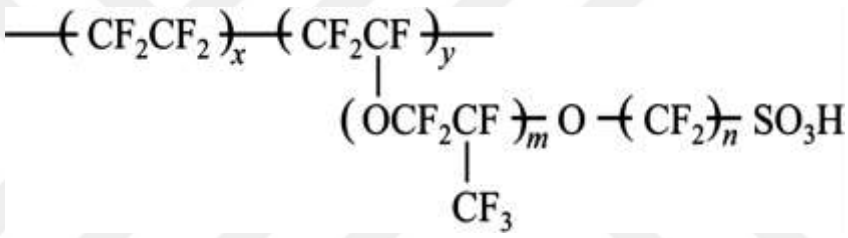

Figure 2.4. Chemical structure of PFSA membrane

The proton conductivity is an important feature of the polymer membrane in the FC. The proton conductivity of the PFSA membrane strongly depends on the structure of the membrane and the humidity condition, therefore, it is extremely hard to sustain a conductivity at a temperature above 90°C [1],[48].

The PFSA membrane has several disadvantages that reduce commercialization, such as low ionic conductivity and low humidity at high temperatures and thus resulting in drying of the membrane [6], [36]. This attributes to the shrinking and cracking of the membrane where it leads to accelerated gas crossover. The O_2 crossover creates the radicals of peroxide and H_2 peroxide, causing the membrane to deteriorate slowly [32].

There are several studies have worked to find an alternative membrane for the Nafion membrane during operation at high temperatures to meet these problems such as PBI [49]. PBI is an amorphous polymer with a high glass transition temperature (Tg

value is between 425 to 436°C). PBI membrane is a good candidate due to its excellent chemical and thermal stability, mechanical strength, durability and low cost [49], [42], [50]. The PBI polymer series is an aromatic heterocyclic group containing units of a PBI. The presence of good mechanical strength is attributed to the H_2 bonding robust between the N and -NH groups [32]. Figure 2.5 shows the chemical structure of the PBI [51].

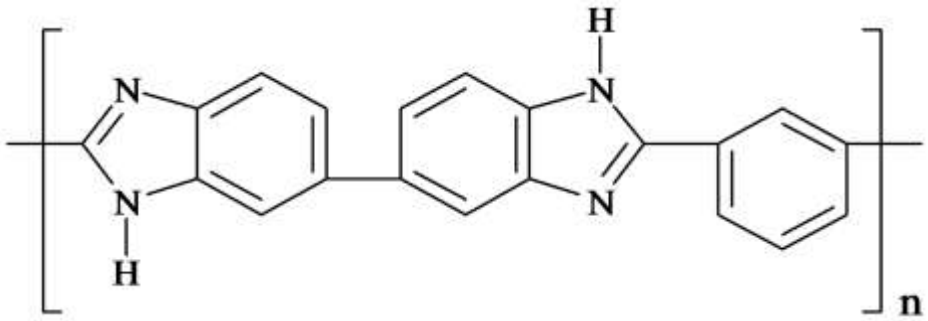

Figure 2.5. Chemical structure of the m-PBI

The PBI polymer membrane has a problem of insufficient proton conductivity and to increase the conductivity needs to be doped PBI with a suitable acid. The conductivity depends on the type and the concentration of the acids. A lot of previous studies have been explained the order of acids, depending on the conductivity as follows: H_2SO_4 > H_3PO_4 > $HClO_4$ > HNO_3 > HCl, at high concentration of the specific doping level. Although sulfuric acid (H_2SO_4) has a higher proton conductivity compared to the other acids, it depends on the moisture content, where it requires 50 % RH. H_3PO_4 is one of the best types of acids that work at high temperatures and it works under the anhydrous suit, does not depend on RH, very good proton conductivity, a more stable thermally at temperatures up to 200°C, and low vapor pressure to reduce evaporation compared to other acids [33], [36], [52], [53].

PBI doped H_3PO_4 also has a high tolerance for contamination, reduces crossover of gas, utilizing waste heat easily, and reduced gas permeability because it is dense [54], [21]. Figure 2.6 shows the chemical structure of PBI doped PA [55].

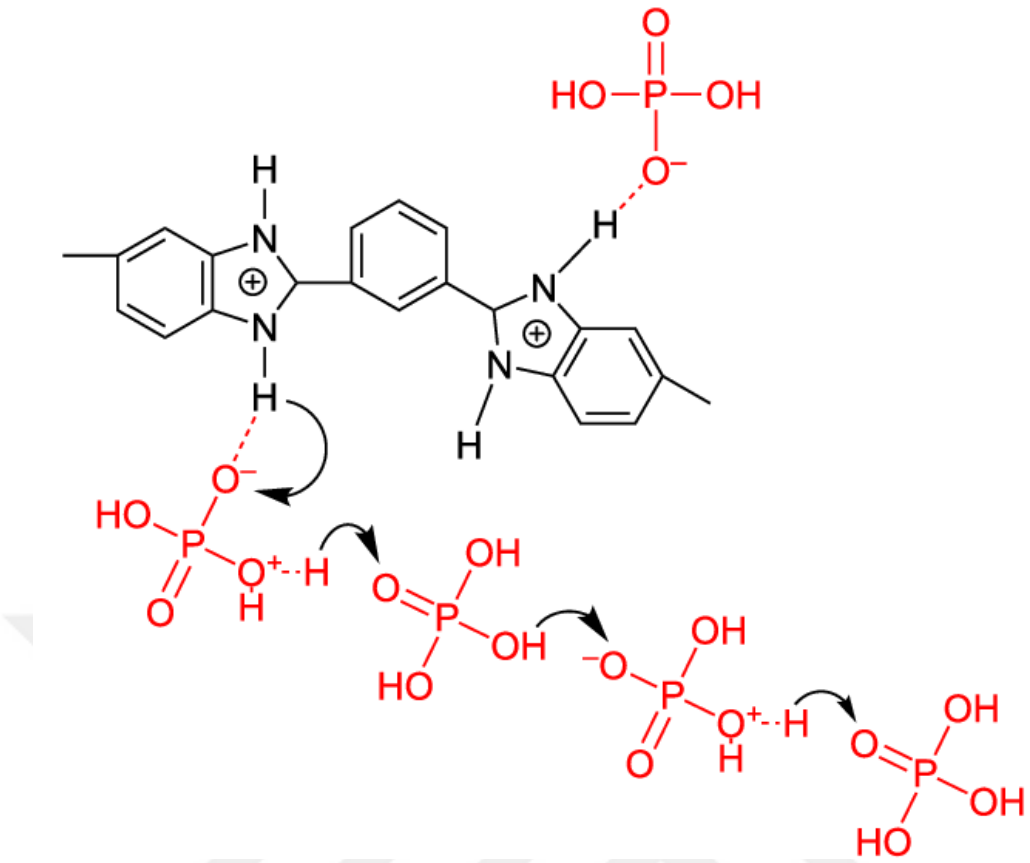

Figure 2.6. Chemical structure of PBI doped PA

There are some limitations facing the H_3PO_4 doped PBI membranes such as low mechanical properties and leaching of an acid from the membrane. To overcome these problems, an appropriate support should be used or by the addition of inorganic fillers where they increase the proton conductivity or acid doping of PBI membranes [48],[49].

Acid doping level is the number of acid molecules per repeating unit of PBI [32]. The higher of the acid doping provide the higher the proton conductivity. The higher acid doping level provides maximum conductivity while maintaining the mechanical strength of a PBI membrane. The weight of the membrane increases after the doping process [36]. High molecular weight is suitable for the investigation mechanical stability and a high acid-doping level, thus lead to high proton conductivity [42]. The only membrane that meets the high temperature PEMFC requirements by the US Department of Energy is defined as the H_3PO_4 doped PBI membrane. The proton conductivity mechanism of H_3PO_4 doped PBI occurs with the "Grotthus mechanism"

[31]. Grotthuss mechanism occurs in a dry atmosphere at the temperature higher than 120°C up to 200°C, rearrange the H_2 bonds between successive molecules [36].

The functions membranes are [4]:

- Allowed H_2 protons to pass through it.
- Prevents the passage of gases through it.
- Good electrical insulation for preventing electrons pass through it.

2.2.2. Catalyst layers (CLs)

The CL is confined between the membrane and the GDL in the membrane electrode assembly (MEA) [56]. The electrode is a thin CL and the main component of MEA of a PEMFC. The electrodes consist of three layers: the backing layer (BL), the CL and the GDL. Some researchers deem the electrodes consist of only two layers, the CL and the GDL, while the GDL layer consists of two layers: microporous layer (MPL) of carbon powder and hydrophobic/hydrophilic agents and a backing layer (BL) composed of carbon paper or carbon cloth [57].

The electrochemical reaction occurs in the CL that connected to the electrolyte membrane, which converts H_2 and O_2 into electricity and water. The CL must consist of catalyst, carbon substrate, hydrophobic material and the ionomer from an electrolyte. The catalyst material provides the stability and the high rate of electrochemical reactions of PEMFC, excludes the use of non- Pt catalysts in PEMFC electrodes while a pure Pt or Pt alloys catalysts are used in both anode and cathode [1], [25].

The three-phase boundary (TPB) is essential to the occurrence of the electrochemical reactions, namely the reaction between the reactant gases, electrons, and protons. The CL should be able to ease the passage of the protons, electrons and gases to catalytic sites [58].

In general, the conductivity in the PEMFC is divided into electrical and ionic. Electrical conductivity is the possibility of the electrode to contact the electron from CL to GDL and then to the BPP. Ionic conductivity is the possibility of the electrolyte membrane connecting H^+ from the anode to the cathode and pass the proton between the CL and the membrane while the gases pass through the spaces,

for this reason the electrodes must be porous to transport the gases. Both connectors have a significant role in PEMFC performance. To improve electrical conductivity in PEMFCs this is done by maintaining pressure [1],[57]. The thickness of the CL ranges from 5-10 micrometers, with porosity 40-70 %, the catalyst should be dispersed with the size of particles 1-10 millimeters. The catalyst loading on the CL is between 0.01 and 5 mg/cm^2 depending on the thickness of the electrode layer. The porosity plays a key role in the transfer of reactant and resulting materials. Porosity also helps regulate the movement between the enter O_2 and the water outside the electrode [57].

The MEA is fabricated in two ways depending on the catalyst deposition method: the catalyst-coated membrane (CCM) and gas diffusion electrode (GDE). There are other techniques for depositing the catalyst such as spraying (manually or using an ultrasound device), rolling, sputtering, screen printing, casting, etc. The spraying method is usually used because it works for a good distribution in the medium [31].

The most important aspects to be achieved by electrodes [1], [57], [58]:

- The electrode should have pores suitable for transport reactant gases.
- The electrode must contain a catalyst that breaks the fuel bonds to form effective ions and protons transported from the anode to the cathode.
- The electrode must connect electrons to the outer circuit.
- It must be electrically conductive and contain a large number of three-phase boundary sites.

2.2.3. Gas diffusion layers (GDLs)

The GDL located between the CL and the BPP [1], [4]. The GDL is usually a double layer of a carbon-based porous material including carbon fiber paper (CFP) or carbon cloth (CC) for the BL layer covered by a thinner MPL consisting of carbon black (CB) powder and a hydrophobic agent. It is available on each side of the electrodes, anode, and cathode [23],[58].

Some researchers are using the back layer (BL) as a support layer for PEMFC. The BL considered a gas distributor and provides a way for electronic and water outside the electrode. The BL must meet several requirements such as high electronic conductivity, hydrophobicity for the discharge of water and facilitate the transfer of

gas to the CL of electrochemical reactions. MPL must possess several properties that have high electrical conductivity, good catalyst support reactions, ability to resist corrosion and the ability to easily restore catalyst properties, and also improves GDL performance. The thickness of gas diffusion materials varies between 0.017 to 0.04 cm, density varies between 0.21 to 0.73 gcm^{-3} , and porosity varies between 70–80 % [1], [57].

When the GDL has the large porosity, the concentration of O_2 increases, the concentration of water decreases from the GDL to the CL, resulting in low-mass transfer resistance of the electrode and create less concentration over-potential. This condition corresponds to HT-PEMFC operating, where the concentration of O_2 and water barely changes due to the low active over-potential of the FC, and the transport of mass in the cathode enhanced. On the other hand, increasing the thickness of the GDL reduces the concentration of O_2 and increases the concentration of water lead to the more concentration over-potential [43].

The most porous GDL, improves cell performance result in a better transfer of reactant to interactive sites. The thinnest GDL optimizes cell performance by reducing the resistance of the mass transfer [31].

The important functions of GDL [1], [25], [58],:

- Distribute H_2 gas to the anode and O_2/air to the cathode, respectively from the BPP to the CL, therefore it must be adequately porous for the flow of reactant and product.
- Supply an electrical pathway for electrons from the BPP to the CL and vice versa, it must be made of material that has good electrical conductivity.
- Removal the heat generated in the electrodes from the CL to the BPP for maintaining the operating temperature of a FC, therefore, it must be thermally conductive.
- A pathway for the water produced by the electrochemical reaction from the CL the BPP, it must be highly porous to transfer the product.
- Provide mechanical support for MEA, therefore it made of material does not degrade after a long hour of the process.
- Provide uniform distribution of gases on the CL.

2.2.4. Bipolar plates (BPP):

The BPP consist of two mono-polar plates on each side, one anode, and the other cathode [25]. The connection of the cathode from one cell to the anode of the following cell electrically called BPP while creating a path for flow reactant gases called flow fields plate [1]. It is also known as the separator plates because of the ability to separate two cells. The cost, weight, and volume of BPP considered an important parameter that has a significant effect on the FC performance where it constitutes a high proportion of the FC cost and weight, estimate about 30 % and 60 % respectively. The BPP has identical functionality to the GDL, both provide distribution of reactant gases and a pathway for electrons [59], [60].

There are several classes of materials used for BPP in FC: metallic materials and graphite including (graphite, composite). BPP is made of the same material for both LT-PEMFCs and HT-PEMFCs. BPP made of metals such as aluminum, steel, titanium or Ni will undergo severe corrosion in the chemical environment of FC, resulting in lower ionic conductivity, increased electrical resistance and the life of FC decreased. While some metals are costly [3], [13]. For these reasons, BPP should be covered to protect the PEMFC from corrosion [1]. Metal plates have mechanical properties and specific weight and Some have sufficient conductivity [13], adequate conductivity so they are preferred for PEMFC transport applications [20].

Thermoplastics are used as materials for graphite composite BPP (such as polypropylene, polyethylene and polyvinyl vinyl fluoride) having a very low electrical conductivity compared to metal plates [1], and poor mechanical strength, facing the problem of high resistance [20].

The BPP are made of graphite [1]. BPP shall be made of high-temperature graphite plates have high electrical conductivity and chemical stability [32]. Graphite plates must be porous therefore cause injurious applications. The process of manufacturing graphite plates is difficult and costly to some applications of FC [1]. The metal plates possess fair conductivity and lack mechanical strength, therefore, is used in composites [13].

Conventionally, non-porous graphite is commonly used as BPP due to chemical and electrochemical stability and high conductivity [20]

BPP must be: [1], [20], [59],:

- Electrically conductive, in order to connect adjacent cells respectively.
- High chemically resistant, to provide adequate corrosion resistance to acids and bases.
- High thermal conductivity, to bind heat from active sites of cells to cold cells.
- Lightweight and good strength, to provide strong structural for the cells in the stack.
- High impermeability to reactant gases, in order to distribute of reactant gases to each side of the MEA and separate the gases in adjacent cells.
- Low cost of material and manufacturing, in order to increase the responsibility of cells in the marketing.
- Able to remove the non-reactant gases and water from the active areas of the MEA.

2.2.5. Gaskets

The FC gasket must possess high stability in an acid environment, good O_2 and H_2 stability, excellent thermal stability, high mechanical strength at low to high temperature, high electrical insulation, sufficient rigidity with adequate processing capability. The gasket material shall be free from diluted ingredients to coat active surfaces of cells and to prevent gas leaks [61].

The main requirements of the gasket are electrical insulation between BPP and GDL. The fitting gasket thickness plays an important role in ensuring gas tightness. Tolerance for changing dimensions during heat cycling and prevent H_3PO_4 from squeeze-out [32]. The gasket works to prevent gas leakage as well as the gas crossover of reactive materials between layers of PEMFC [23],[62]. The gasket keeps the MEA components together also works to reduce the contact resistance between these layers [1]. The gasket also controls the stack height [50].

The gasket of a FC is made of different materials ranging from rubber to polymer [1]. Basic rubber includes silicone, fluoropolymers, or hydrocarbons [50]. Silicon also called polydimethylsiloxane (PDMS) is used as a gasket material at a high temperature better compared to Teflon as a result of uniform distribution and resistance to leakage [63], [64]. Although the silicone rubber has sufficient thermal

resistance, it suffers from poor chemical resistance under acidic medium and it is more expensive than other types of rubber [61]. The use of ethylene-propylene-diene-monomer (EPDM), butyl rubber (IRR), or fluoroelastomer (such as Viton) is the best [50]. EPDM is a polymer that has a good heat resistance and cost effectiveness but has low elasticity and thermal resistance compared to fluoroelastomer [61]. On the other hand, Polytetrafluoroethylene (PTFE) has tightness of gas and good chemical stability so it is used as a gasket at high temperatures [32]. While using the Viton as promising candidate gasket for high temperature [65]. Viton gasket is preferred for use at high temperatures between cell layers due to its high mechanical and high thermal resistance [27].

2.2.6. End Plates

End plate made of various materials such as stainless steel at high temperatures [33]. End plate located outside the stack where it used to provide appropriate internal compression and fasten the structural components of the FC to a set of bolts and nuts or another fixation mechanism [4],[66].

The clamping force is equal to the force in demand to compress the gasket plus the force required to compress the components of the stack, plus internal force [1]. The use of non-uniform pressure or insufficient pressure will cause stack problems leading to fuel leakage, internal combustion and unacceptable contact resistance. Increasing the pressure above the limiter damages the FC layers and thus reduces cell performance and catalyst degradation. Each stack has a unique assembly pressure where the end plates are fastened by the clamping device. The selection of suitable clamping force is very important in stack design to achieve the optimal performance of the PEMFC [67].

The optimized design of the end plate is very necessary to improve the efficiency, reliability, and performance of PEMFC. Anxiety for design is an important indicator for PEMFC and avoiding the irregular distribution of pressure due to the deviation at the end plate. Mechanical integrity and proper rigidity of the end plate also very necessary [68]. High hardness can be accomplished for the end plate by increasing its thickness, but this leads to a large mass and size. To reduce mass and provide high

rigidity, this is achieved in complex configurations such as ribbed-, bomb-, or bow-shape [66].

The end plate should provide a uniform and sufficient compression of stack components because adequate pressure on the stack is very important to prevent fuel leakage and to minimize the electrical contact resistance between stack components. The uniform distribution of pressure is also necessary for the safety and efficiency of PEMFC. The end plate should also provide good heat insulation and high thermal resistance in order to prevent heat loss during operation and thus improve the cold start properties of PEMFC [68].

The average contact pressure and the contact pressure distribution are very affected by the placed on the bolts. The placement of the bolts through the graphite plate contributes to the uniformity of the pressure distribution [69].

2.3. Bimetallic Catalysts

Bimetallic catalyst is the process of incorporating metal types with parent metal such as metal Pt for the purpose of reducing cost, improving the activity and stability. Bimetallic catalysts exhibited higher catalytic activity than pure catalysts, changing the electronic structure of metals and adjusting adsorption energy as well as thermodynamic stability. In the past decades, bimetallic systems have received considerable interest in heterogeneous catalysis. The advantages of the bimetallic catalyst for ORR in the PEM were observed [70], [71].

The catalyst is used in the reaction and it is not consumed during the reaction, it works to accelerate the reaction. The best catalyst used in PEMFC is Pt metal because of its high current density, high catalytic activity and outstanding work function [5], [72].

Although Pt is the best catalyst for HOR and ORR, it still suffers from some constraints that obstacle the commercialization of PEMFC applications such as high cost, which amounted from $ 20 to $ 50 approximately per gram in 1960-2014 [36], poor stability in particular, very limited resources [73], [74]. In addition, the Pt catalyst for HT-PEMFC sometimes suffers from some degradation due to the dissolution, the aggregation or separation of the nanoparticles of Pt catalyst [36].

The most important challenges that limit the commercialization of the PEMFCs are durability and cost, 55 % of the cost of PEMFCs return to the Pt catalyst [65]. To reduce the loading of the Pt and improve stability is achieved by introducing second metal into the parent metal (Pt) without compromising the activity and efficiency to adjust the electronics and surface effects and enhance physical and chemical properties [74], [75]. The Palladium (Pd) is a more suitable metal that used in the manufacture of the bimetallic catalyst with Pt because of their [76], [74]:

- Similar lattice structure face-centered cubic (FCC).
- Matching lattice [slight discrepancy (of only 0.77 %)].
- Good blending for Pt-Pd formation.
- Same periodic group.
- The cost of Pd is much lower than Pt (about one-third only).

Reduce durability does not mean occurrence a disaster, but it causes an irreversible loss of performance. Durability affects performance during the long-term operation as the catalyst activity and certain properties change as a result of the erosion of carbon support [22]. To avoid the degradation of the catalyst and enhance the durability, it is necessary to use the catalyst support because the catalyst support improves stability and high activity. Each support material has a different effect on performance. Suitable support with specific surface area (SSA), low flammable, high stability, excellent corrosion resistance, good electrical conductivity. Support materials play an important role in finding the performance and durability of PEMFC. The compatibility between support and catalyst reduces the losses of the catalyst activity, improves the efficiency and durability of the catalyst. CB is one of the materials widely used as a support for PEMFC because many properties have a high surface area and electrical conductivity, but black carbon increases the corrosion rate of the cell as it hinders the stable operation of FC [34], [77].

Carbon corrosion causes the weak attachment between the catalyst and the carbon support. This results in Pt agglomeration or loss of Pt mass during prolonged operation [32]. The reduced SSA due to increased carbon corrosion then increased particle size leads to performance losses in the catalyst. Carbon corrosion serves to form surface groups by imperfect oxidation. Increasing the catalyst particle size leads

to reduced dispersion and increased agglomeration thus cause loss of activity of the catalyst [22].

CB does not meet all operating conditions requirements. Several efforts and studies have been undertaken to find alternative support to meet all FC operating conditions. The search for alternative catalyst support works to develop efficiency, lower cost and high durability lead to the successful marketing of cells is important and essential. Among the supported types, carbon nanotube (CNT) are deemed more interested and convenient due to its high crystallinity, lightweight, perfect hexagonal structure hydrophobicity, excellent tensile strength, high thermal and electrical conductivity, chemically inert, high surface area and good properties in electrochemical reactions. CNT also works to improve stability, reduce the surface oxide formation and corrosion stream [14], [65], [78], [79].

CNT appears as one-dimensional carbon, consists of single walled CNT (SWCNT) and multi walled CNT (MWCNT). SWCNTs consists of one tube of graphene (G) while MWCNTs consists of several tubes of concentric G intertwined with each other [80]. MWCNT has a higher performance and durability than SWCNT. As a result of the advantages of MWCNT is considered the best support candidate promising for the PEMFC. MWCNT is used as catalyst support, attracting the attention and attraction of scientists as a promising candidate because the deposition of nanoparticles of the catalyst is distributed uniformly on the surface of MWCNT so it prevents aggregation and thus improves catalyst activity. Nitrogen doped MWCNT (N_2-MWCNT) is used as a catalyst support for HT-PEMFC because N_2 has effective sites. [36], [79].

On the other hand, G is the same as CNT, where CNT consists only of carbon atoms, while G is a two-dimensional (2D) flat sheet [81], G have attracted considerable interest as the catalyst support. G is the important support due to high electrical conductivity, a unique property for electron transport, high surface area, improved catalyst activity, performance and efficiency as well as improved durability [21], [82]. G nanoplatelet (GNP) is a stack of G sheets, whose thermal and mechanical properties are similar to CNT, GNP has received great attention due to its superior mechanical, thermal and electrical properties which are two-dimensional (2D). GNP has very high conductivity and corrosion resistance. Also, it has a higher aspect ratio

compared to CNT. GNP dispersion is easier compared to CNT as well as less expensive GNP contains a 10-30 stack layer of G compared to monolayer G. GNP has uniform dispersion and distribution as well as the interaction between it and the other compound [83],[84].

As a result of the characteristics of GNP, therefore the contact of it with CNT results in superior properties. Hybrid MWCNT doped GNP (MWCNT-GNP) together, resulting in the formation of three-dimensional hybrid structures where they prevent their aggregation as they produce a high contact area between them [85]. MWCNT-GNP hybrid support material showed better dispersion than both GNPs and MWCNTs alone. MWCNT-GNP conductive charges possess unique structures and superior conductivity [86]. The presence of CNTs with GNPs can reduce the re-stacking problem for GNPs by accessing the gap between G papers. It is possible for GNPs to wrap with CNTs where the CNT agglomeration is prevented. The combined of the effect of CNTs and GNPs resulting in an improved hardness composite and improved mechanical properties [87].

The catalyst interaction process with support helps transfer the electron from the Pt group of the O_2 atoms and also improves the stability of the catalyst [21]. It is important to choose a suitable method to achieve the best efficiency and performance of the catalysts. There are many techniques used to prepare Pt:Pd catalysts for PEMFC such as plasma-assisted deposition [88], microemulsion method [89], dry impregnation [90], facile hydrothermal method [91], facile one-pot wet-chemical [92], simple chemical deposition [93].

One of the most important techniques used in the preparation of the bimetallic catalyst is the microwave assisted synthesis, which possesses several superior advantages compared to conventional heating, such as, energy transfer instead of heat transfer, volumetric heating, rapid start-up and stopping [94], homogeneity of reaction [95], low cost, easy temperature control [96], fast heat within a short period [97].

Microwave-assisted synthesis is a method that uses electromagnetic energy at frequencies ranging from 300 MHz to 300 GHz. The rate and efficiency of microwave assisted heating rely on the ion conductivity and bipolar interactions

between materials and microwave where the polar ends generate heat as a result of cracks generated by the partial collision to swing in an electric field [98]. Microwave method provides uniform distribution of particles due to water molecule stirring owing to electromagnetic field [99]. The chemical composition of nanocrystals is well controlled by microwave by adjusting the ratio of precursor and concentrations as well as the microwave conditions. Some of the major challenges to microwave synthesis must be handled. Control the size, composition and morphology of the microstructure, and collect nanostructures of the microwave synthesized. The use of the microwave oven should be controlled to avoid the risk of explosions [100]. Polar solvents are important factors in microwave synthesis. Ethylene Glycol (EG) that is odorless, colorless, sweet, is used as the liquid polar solvents in the microwave and it reduces agent at the same time. EG decomposes when heated and minimizes metal ions into metal particles [101], [102]. PH is an important factor and a strong influence on microwave because Pt load is decreases when pH is increasing [101]. It is necessary to achieve durability using microwave synthesis, where exposure to carbon and precursors in the microwave method is reduced due to short processing time as it affects the interaction of nanoparticles [22]. On the other hand, the addition of support to the synthesis mixture helps to precipitate the nanoparticles directly on the support, which improves stability and thus performance [101]. Due to the advantages of microwave assisted technique is deemed as a promising preparation method that improves the durability of PEMFC. The better dispersion of metal nanoparticles on appropriate support and suitable catalyst synthesis method is essential to improve catalyst activity and stability as well as the durability of the bimetallic catalyst and thus leading to improve the performance.

There are several literature studies summarized in Table 2.2, for the different catalysts and methods of manufacture in addition to the precursor base materials and characterization method. Although there are some studies about ORR comparisons using different catalyst support materials with Pt:Pd in the literature, HER comparison is quite limited. Zapata-Fernandez et al. studied the effect of the Pt:Pd/MWCNT catalyst on ORR in PEMFC applications. They observed the highest catalytic activity with the lowest Pt load [103]. Bharti and Cheruvally explained that when MWCNT supported Pt:Pd with existence the anionic (SDS) and cationic (CTAB) surfactant or absence surfactant and its effect on the ORR. They showed

when there is SDS produces MWCNT desegregation with uniform dispersion that is similar to MWCNT without surfactant leading to enhance the performance of ORR [76]. Zhong et al. employed bifunctional electrocatalyst for hydrogen evolution reaction (HER) and ORR using Pt:Pd/NPG, where high-efficiency bi-function was detected for both HER and ORR due to use G [104]. Kang et al. suggested the synthesis of Pt:Pd support on the G-MWCNT hybrid material for ORR and compared with the mono catalyst Pt support of G and G-MWCNT. They observed that the Pt:Pd support on G-MWCNT has high activity and improved durability towards ORR compared to mono catalyst Pt support on G and G-MWCNT [105]. Limpattayanate and Hunsom have studied the effect of different support material types for Pt:Pd for ORR in PEMFCs. They found that Pt:Pd/Vulcan XC-72 gives maximum ORR activity [106]. Nguyen and Shim achieved that the activity of ORR enhanced and stability, by synthesis Pt-Pd nanoflowers supported on carbon in 0.1 M perchloric acid ($HClO_4$) solution by using the simple wet method [107]. Xiong et al. explored that Pt:Pd nanodendrites support on carbon improves the performance and durability of PEMFC. It also eases the transfer of electrons, protons, and O_2, which enhances ORR activity due to alloy synergy compared to Pt/C catalyst [108]. Daş et al. worked Pt catalyst support GNP by two different methods supercritical carbon dioxide (scCO2) deposition and microwave assisted synthesis methods. They demonstrated more enhancement to the catalyst and better cell performance compared to the commercial catalyst [109]. Jafri et al. proposed Pt particles on GNP for ORR in PEMFCs applications. They showed that the performance of Pt/N-G enhanced compared with Pt/G due to enhancing catalyst-carbon binding where the N_2 provides good sites for nanoparticle deposition and increases electrical conductivity [110]. Ramakrishna et al. used the chemical reduction method for the preparation of Pd catalyst support on N-CNTs towards H_2 evolution reaction which shows the higher electrochemical activity compared to Pt/C due to a better structure of electrocatalyst [111]. Devrim and Albostan have reported the synthesis of Pt catalyst support on G by chemical reduction. They showed that the Pt/G showed better stability and durability for PEMFC compared to Pt/C catalyst and thus the performance and current densities improved [112]. Bharti et al. prepared Pt/CNT with two different methods of microwave assisted synthesis and conventional heating by using $NaBH_4$ and EG as reducing agents. They found that the microwave assisted

method exhibit high performance for ORR at cathode due to homogeneous dispersion and small size of Pt particles [113]. Moreira et al. studied the synthesis of Pd/Vulcan and Pd/C catalysts by the impregnation method in the PEMFC and compare between them. They observed that the Pd/Vulcan catalyst is better than Pd/C to improve the ORR [114]. Erikson et al. Pd deposited carbon glassy catalysts for ORR were prepared through the rotating disk electrode method in acid and alkaline solutions. Which showed the electrodeposited Pd more active for ORR in alkaline than acid [115].

In this study, Pt:Pd bimetallic catalyst support on different support materials as GNP, MWCNT, and MWCNT-GNP were prepared by microwave assisted synthesis method. In literature, there are lots of different catalysts used for HT-PEMFC application; nevertheless, best to our knowledge, the HT-PEMFC performance of Pt:Pd supported MWCT-GNP, GNP and MWCNT catalysts was depicted for the first time in the literature by this work in detail. The structural characterization of the catalysts characterized by thermogravimetric analysis (TGA), X-ray diffraction (XRD), transmission electron microscopy (TEM), and Inductively coupled plasma-mass spectroscopy (ICP-MS). The electrochemical characterization of the prepared catalysts was examined by the cyclic voltammetry (CV) method. The results showed that Pt:Pd/MWCNT-GNP has better durability and HT-PEMFC performance compared to catalyst supported by GNP, MWCNT due to uniform dispersion and smaller crystallite size in addition to effective interaction between MWCNT-GNP hybrid support material. Results also showed that the microwave assisted synthesis technique is a promising preparation method that improves the durability.

Table 2.2. Comparison of different catalysts for PEMFCs applications

Support	Catalyst name	Synthesis method	Applications	Characteristic method	Initial materials for synthesis	References
MWCNT	Pt-Pd	Galvanic displacement (GD)	ORR	TGA, ICP-OES,TEM, CV RDE, EIS, HAADF	K_2PtCl_6, Na_2PdCl_4	[103]
CNT	Pt-Pd	Microwave assisted	ORR	XRD,ICP-AES,XPS, BET, CV, FESEM, HRTEM ,EIS	K_2PtCl_6, $PdCl_2$	[76]
N2 rich G	Pt-Pd	Hydrothermal process	ORR, HER	TEM, HAADF-STEM, EIS, CV, EDX, SEM, XRD, TGA, RDE, XPS, BET	PtPc, PdPc	[104]
G-MWCNT	Pt-Pd	Facile surfactant free and template free	ORR	SEM, STEM ,HAADF, EDS, TEM, XRD, XPS, RDE, CV, ICP-AES	$H_2PtCl_6.6H_2O$, $PdCl_2$	[105]
Vulcan	Pt-Pd	Impregnation and seeding	ORR	BET, XRD, SEM, RDE SEM-EDX	K_2PtCl_6, $PdCl_2$	[106]
C	Pt-Pd	Simple wet chemical	ORR	TEM, XPS, EDS, SEM, XRD, ICP-OES, HAADF-STEM, CV, RDE	H_2PtCl_6, Na_2PdCl_4	[107]

Table 2.2. Continued

Support	Catalyst name	Synthesis method	Applications	Characteristic method	Initial materials for synthesis	References
C	Pt-Pd	Facile Solvothermal	ORR	XRD, TEM, HRTEM, CV, XPS, ICP-AES, EDX, RDE	Pt(acac)2, Pd(acac)2	[108]
GNP	Pt	Microwave irradiation & scCO2 method	ORR	XRD, TGA, TEM, CV, PEMFC Test	H_2PtCl_6	[109]
N2 doped GNP	Pt	Convectional Chemical reduction	ORR	XRD, XPS, TEM, RS Fuel cell test	H_2PtCl_6	[110]
N2 doped CNT	Pd	Chemical reduction	HER	FESEM, XRD, CV, SEM, EDX	$PdCl_2$	[111]
G	Pt	Chemical reduction	ORR	TGA, XRD, SEM, EDX, FC test	H_2PtCl_6	[112]
CNT	Pt	Microwave assisted and conventional heating	ORR	XRD, HRTEM, TGA , XPS, ICP-AES, BET, CV, RS, EIS	$H_2PtCl_6.6H_2O$	[113]
Vulcan	Pd	Impregnation method	ORR	XRD, TPR, AAS, RDE, CV	Pd(acac)2	[114]
Gc	Pd	Rotating disc electrode (RDE)	ORR	HRSEM, CV, SEM	$PdCl_2$	[115]

CHAPTER 3

3. EXPERIMENTAL STUDIES

3.1. Materials

Chloroplatinic acid hexahydrate ($H_2PtCl_6.6H_2O$) and Palladium (II) chloride ($PdCl_2$) which used as metal precursors, were purchased from Sigma-Aldrich. 3,3'-Diaminobenzidine (DAB), terephthalic acid (TPA), polyphosphoric acid (PPA) (115 % phosphoric acid equivalent), Ethylene Glycol (EG), ($HOCH_2CH_2OH$), isopropyl alcohol ($CH_3CH(OH)CH_3$, IPA), N-N dimethylacetamide ($CH_3C(O)N(CH_3)_2$ (DMAc), H_3PO_4, (85 %), Deionized water (DI), acetone (C_3H_6O), Perchloric Acid ($HClO_4$), sodium hydroxide (NaOH) and nitric acid (HNO_3) were obtained from Sigma-Aldrich. MWCNT, GNP and Multiwalled Carbon Nanotube Doped GNP (MWCNT-GNP) used as support materials were taken from Nanografi. All gases which were used in the experiment having high purity (>99.98 %) were purchased from Linde. PBI polymer was used as a binder. The commercially available GDL that employed as anode and cathode, was obtained from Freudenberg, Germany.

3.2. Membrane Preparation

Firstly, PBI polymers were synthesized in our laboratory for membrane preparation. The polymers were synthesized according to the solution polymerization method under the flow of nitrogen at 200°C for 18 hours in our laboratory by our team [49]. The synthesis set up includes calcium chloride ($CaCl_2$) drying tube, heating mantle, a four-neck glass bottle, nitrogen inlet, and mechanical stirrer. After PBI polymers were synthesized, the membranes were prepared according to the solvent casting method [116]. 5 wt. % PBI polymers were dissolved in DMAc at 60^oC, then the solution was cast onto a glass plate.

The DMAc was started to evaporate from the solution in an oven at 80^oC for 12 h, then the membrane fully dried at 130^oC for 12 h. Thickness of the membrane was

around 55 ± 5 μm. Then the PBI membrane immersed in H_3PO_4 during two weeks. The weight of the membrane was measured before and after the immersion to calculate the H_3PO_4 based weight gains of membranes. The acid doping ratio is important for the proton conductivity and the acid ratio can be decreased with produced water inside the HT-PEMFC. To calculate the amount of acid retention, acid leaching test was made as described in a previous study [117]. The membrane was kept in water vapor and the weight loss due evaporation of H_3PO_4 was calculated during five hours by weighing the membranes every hour. The acid doping level and acid loss percentage equations are given in APPENDIX A .

3.3. Catalyst Preparation

The catalysts were synthesized by the microwave assisted method following the procedure described in the previous study [65]. Firstly, the support materials (75 mg) dispersed in a mixture of EG (36 ml) and IPA (9 ml) by volume ratio (4:1), with an ultrasonic bath for 60 min. EG is a viscous liquid of moderate toxicity used as a reducing factor to convert metal ions into the nanoparticles for metals or alloys, stabilize metals and it is used for antifreeze additive, while IPA used to adjust the viscosity [44], [102], [118]. Then, $H_2PtCl_6.6H_2O$ and $PdCl_2$ were added to the solution at the calculated 50:50 molar ratio to contain 40 % metal in the catalyst. The solution mixed in the ultrasonic bath for 10 min. The pH of the solution was increased to about 12 by adding 1 M NaOH into the EG solution. The resulting solution was placed in a microwave oven. The microwave oven worked for 600 W during 60 s. The working parameters were chosen from the parameters showing the best results in the previous study [65]. After the microwave process, the pH of the solution was decreased until reaching around 2 by adding 0.2 M HNO_3. The resulting mixture was filtered, washed with acetone, and dried in an oven at 100 °C overnight.

3.3. Catalyst Characterization

3.3.1. Structural Characterization

3.3.1.1. Thermogravimetric Analysis (TGA)

TGA is a method used to measurement of the weight of the materials as a function of temperatures. TGA is used to study thermal stability of the catalysts. TGA method is shown as a region of weight loss due to oxidation, degradation or the loss of volatiles [24]. TGA method is also used to determine the metal loading of the catalysts. TGA was conducted at a ramping rate of 10°C/min under the air atmosphere on a Perkin Elmer Pyris 1, from room temperature to 900°C [119].

3.3.1.2. X-ray Diffraction (XRD)

XRD technique was used extensively to observe the crystallite structure of the catalysts. XRD is also can used to calculate the average crystallite size of catalysts. When X-rays interact with catalyst samples, the nanoparticles of the catalyst are scattered. XRD values of catalysts were measured on a Rigaku Ultima-IV device using Cu Kα (λ = 1.5406 A^o) radiation source which is performed between 20–60 kV and 2-60 mA with angle 10^o-90^o [65], [98].

3.3.1.3. Transmission Electron Microscopy (TEM)

TEM is an electron microscope that is comparable to a light transfer microscope, but the TEM uses a concentrated beam of electrons to analyze catalyst samples in order to obtain the physical and chemical structures of nanoparticles. TEM provides rich information on morphology, structure and chemical composition and provides the size, shape and distribution of nanoparticles [31], [70]. The structure particle sizes distribution of Pt:Pd on the supports were described by JEOL 2100 JEM device.

3.3.1.4. Inductively Coupled Plasma-Mass Spectrometry (ICP-MS)

ICP-MS is a method for analysis of the elemental and isotopic structure. The solutions are sprayed to the ICP-MS. Then the obtained ions transferred to the differentially pumped interface into a vacuum system which has a quadrupole mass spectrometer [120]. This technique is used to examine the amount of Pt and Pd, so their ratio in the bimetallic catalyst by controlling the precursor composition the analysis was performed by Perkin Elmer DRC II device [27], [121].

3.3.2. Electrochemical Measurements

3.3.2.1. Cyclic Voltammetry (CV)

CV is an effective method for identifying electrochemical active surface areas (ECSA) of catalysts and carbon corrosion of the catalyst, [22], [82]. CV measurements were performed with a potentiostat (Wonatech ZIVE-SP2 Potentiostat/Galvanostat/FRA) using a three-electrode system that has the working electrode (WE), the reference electrode (RE), and the counter electrode (CE). In this study, a glassy carbon (GC) disk electrode (0.0707 cm^2), Ag/AgCl filled with saturated sodium chloride (NaCl) solution, and the Pt coil were used as the WE, the RE, and CE, respectively. Before preparing the electrode, the glassy carbon electrode was polished with a 0.1 μm diamond solution until the mirror finish was acquired. The catalyst ink was prepared by dispersing the catalyst in the IPA (0.25 ml), DI (0.75 ml) and polymer solution (0.005 ml) with an ultrasonic bath for an hour. After mixing process of the catalyst ink, 2 μl ink loaded on the working electrode to obtain 21 $\mu g/cm^2$ catalyst loading and dried overnight at room temperature. The CV measurements were performed at 25°C with 200 mV/s from - 0.25 V to -1.2 V in a 0.1 M $HClO_4$ electrolyte solution for 1000 cycle. Before the CV measurements, the electrolyte solution was purged with N_2 for 30 min to remove O_2.

3.4. Membrane Electrode Assembly (MEA) Preparation

The ultrasonic coating technique was used for the manufacturing of gas diffusion electrodes (GDEs) that would be a component of PBI based MEAs tested within the scope of the thesis. The catalysts were homogeneously coated with the ultrasonic coating technique with little catalyst loss [122]. The HT-PEMFC catalyst ink was prepared by using the method as described by Devrim [48]. Catalyst ink includes of 70 wt. % prepared catalyst, 5 wt. % PBI solution and DMAc. The mixture was mixed in the ultrasonic bath for 40 minutes before the coating. The catalyst inks were filled to a syringe pump prior to atomization in the nozzle and sprayed to GDLs use a flow rate of up to 0.5 mL/min to give a catalyst loading about 1 mg/cm^2. This solution was ultrasonically sprayed on the commercial carbon papers which used as GDL by an ultrasonic spray coater (ExactaCoat, Sono-Tek) with 120 kHz Impact Nozzle (Figure

3.1) by keeping the GDLs on a heated plate at 80^{o}C. The coating process was carried out with the control of a computer specially programmed for the coating area.

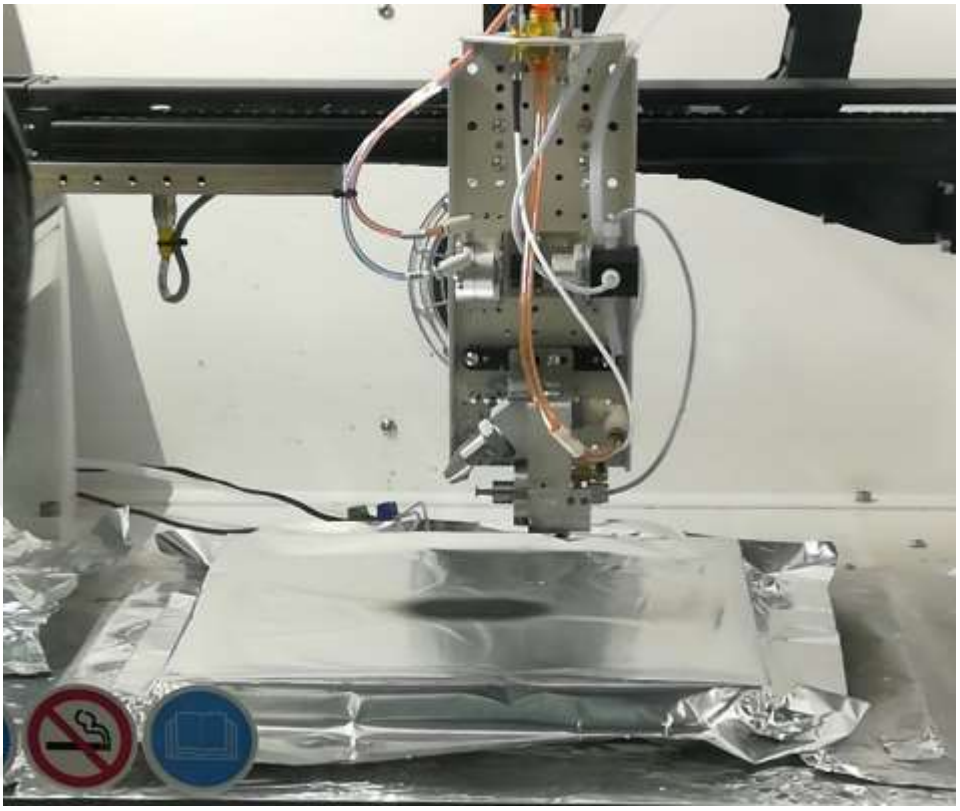

Figure 3.1. GDL coating process

Finally, the produced GDLs were pressed with the H_3PO_4 doped PBI membranes at 150°C and 172 N/cm^2 pressure for 5 minutes by a hot press at Atılım University Hydrogen Energy and Fuel Cell Research Laboratory (Figure 3.2).

Figure 3.2. Hot press

3.5. HT-PEMFC Tests

The HT-PEMFC test station using in our laboratory shown in Figure 3.3. Performance tests of the HT-PEMFC were done with an electronic load (BK Precision, USA) and test station software computer. The mass flow controller (MFC) parameters, temperature indicators and controllers, valves and HT-PEMFC' current and voltage parameters were pursued and controlled during the operation by the test station control and data acquisition software.

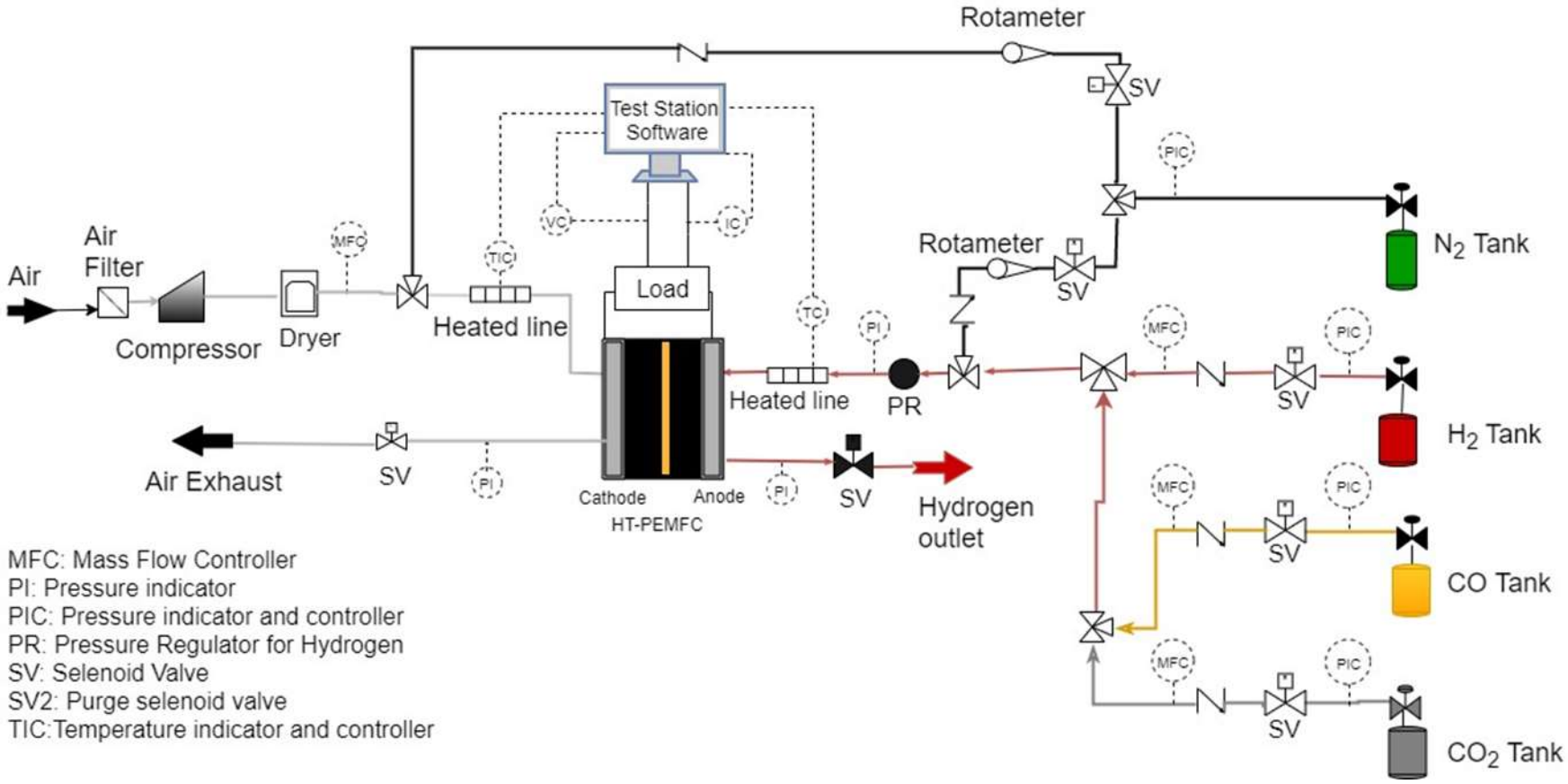

Figure 3.3. HT-PEMFC Test Station Flow Chart

H_2 tanks outlet pressure controlled with the regulator. After the tank, H_2 or reformate gas were controlled through the MFC, valves, heater, temperature indicator and controllers before entering the anode side of HT-PEMFC. For the cathode side of HT-PEMFC, first air filtered and then fed to the dryer and heater with the aid of a compressor. The dryer was used to prevent loss of H_3PO_4 in the membrane structure by liquid water. The three-way valves of N_2 line were used to feed N_2 to the leakage test and system cleaning, before and after the experiment.

Before the single cell performance experiment, the heated gas lines were heated until 120°C. When the heated lines reach 120°C the single cell heated to 160°C. When the desired values are reached, mass flow rates of H_2 and the dry air were arranged. To condition the MEA, the cell was maintained at a constant voltage of 0.7 V for 12 hours. After conditioning, single cell performance results were measured for different voltage values.

In the cell closure method, the single HT-PEMFC voltage was set to OCV. After the cell was cooled down to 120^{o}C, the current draw was terminated, and N_2 was passed through the system and the system cooled to room temperature.

CHAPTER 4

4. RESULTS AND DISCUSSIONS

4.1. Structural Characterization

The TGA curves of our synthesized catalysts are given in Figure 4.1. From this figure, catalysts showed different regions for the weight loss they were various for each catalyst.

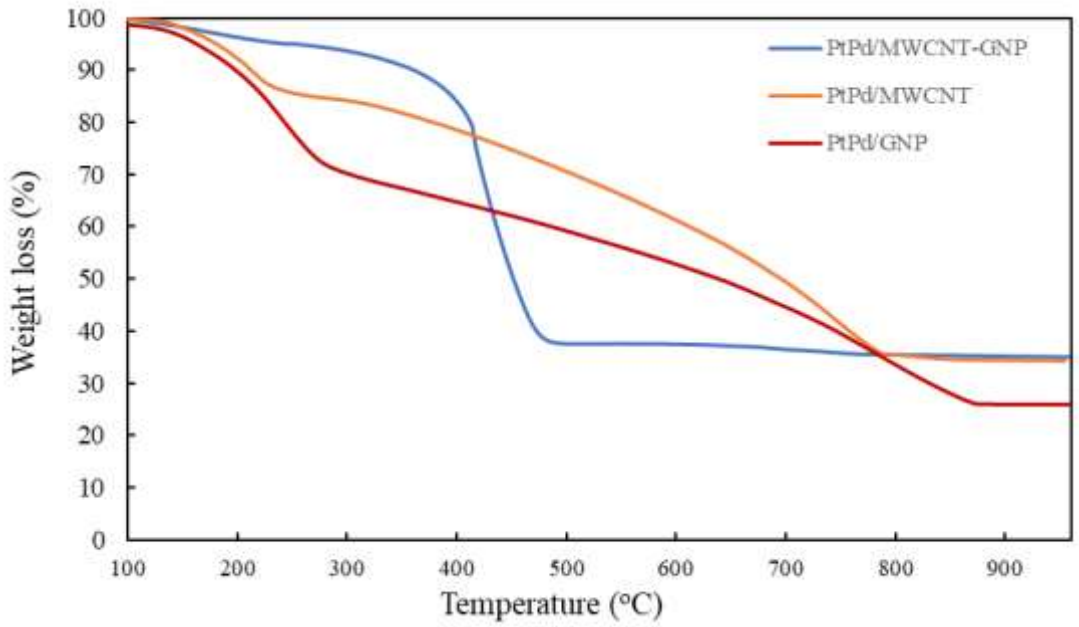

Figure 4.1. Thermal behavior of the Pt:Pd/MWCNT-GNP, Pt:Pd/MWCNT and Pt:Pd/GNP catalysts

The first mass loss region occurred until 250-280°C, can be attributed to the ease of elimination of the volatiles of compounds and water absorption. The second mass loss region takes place at the range temperature between 250-780°C, 250-480°C, 280-850°C for Pt:Pd/MWCNT, Pt:Pd/MWCNT-GNP and Pt:Pd/GNP, respectively. The region can probably be ascribed to the decomposition of the thermal support.

The final mass loss region is a temperature range of 780-900°C, 480-900°C and 850-900°C for Pt:Pd/MWCNT, Pt:Pd/MWCNT-GNP and Pt:Pd/GNP, respectively. The results showed that the support material could be decomposed at much lower temperatures when using it as a hybrid. Nevertheless, this low temperature does not affect the working condition as it is far above the operating temperature of HT-PEMFC. Finally, the Pt:Pd loadings of the catalysts were calculated from the point at which the TGA curves are fixed (Table 4.1). According to results, Pt:Pd/MWCNT-GNP has higher metal loading and thermal stability than the other support material.

TGA and ICP analysis results are given comparatively in the Table 4.1. According to the results obtained, metal loads obtained by ICP and TGA analysis were found quite close. ICP-MS analysis was also confirmed the total metal loading of the catalysts. The composition of these catalyst was found to be $Pt_{60}Pd_{40}$/GNP, $Pt_{52}Pd_{48}$/MWCNT and $Pt_{58}Pd_{42}$/MWCNT-GNP by ICP analyses. The amount of metal in the mass ratios of the bimetallic catalysts prepared was little bit higher than the targeted ratio. This may be due to the fact that the precursors Pd are not completely reduced to the metal Pd or that the precursors Pt is higher [123].

Table 4.1.Pt:Pd loading of prepared catalysts according to TGA and ICP analysis.

Catalyst Name	Pt:Pd loading by TGA (%)	Pt:Pd loading by ICP-MS (%)
Pt:Pd/GNP	27.3	26.2
Pt:Pd/MWCNT	34.5	35.0
Pt:Pd/MWCNT-GNP	35.1	38.9

XRD patterns of the catalysts, shown in Figure 4.2. The Pt:Pd/GNP catalyst displays three peaks at 2θ values of 26.63^o, 29.403 ^{o}, 31.76 ^{o}, corresponding to (002) planes and a peak at 2θ is 47.935^o, corresponding to (101) plane of the graphite structure. The rest of the characteristic diffraction peaks were observed at 2θ values of 39^o, 39.95^o, 46.28^o, 68^o and 82.04^o corresponding to the (111), (111), (200), (220), and (311) planes of the FCC structure of Pt:Pd catalysts, respectively. The first peak of Pt:Pd/MWCNT catalyst showed at the 2θ value of 25.87^o correspond to (002) planes

of graphite structure, whereas other distinctive peaks of XRD patterns of catalysts were observed at 2θ values of 40.03°, 46.5°, 68.03° and 81.84° corresponding to (111), (200), (220), and (311) planes of fcc structure of Pt:Pd catalyst, respectively. Also a peak at the 86.7° for Pd fcc structure corresponding to (222). The catalyst Pt:Pd/MWCNT-GNP showed the first peak at the 2θ value of 26.10° correspond to (002) planes of graphite structure, while the other characteristic diffraction peaks of XRD patterns of catalysts were observed at 2θ values of 40.03°, 46.56°, 67.74°, and 82.83° corresponding to (111), (200), (220), and (311) planes of fcc structure of Pt:Pd catalyst, respectively.

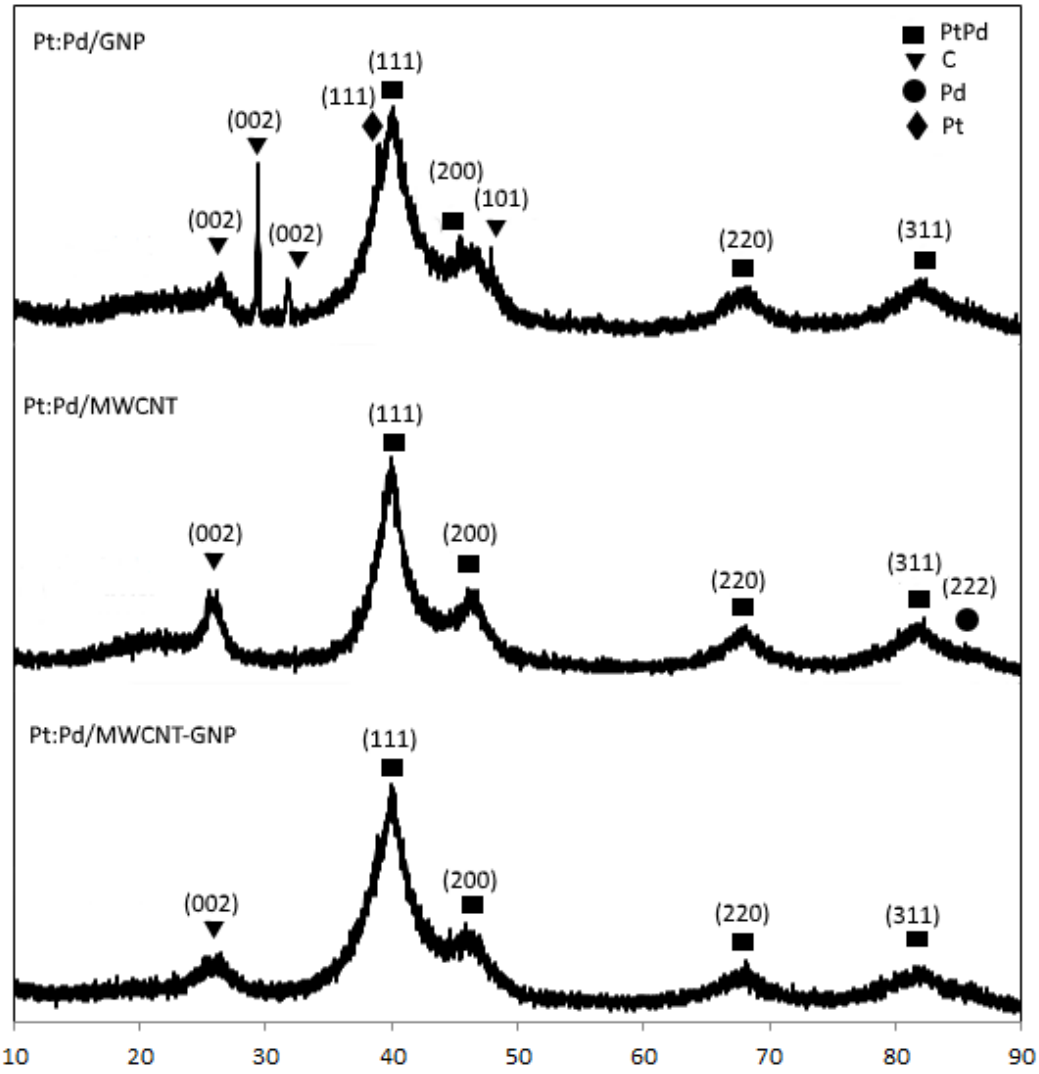

Figure 4.2. The XRD patterns of Pt:Pd catalyst support on GNP, MWCNT, and MWCNT-GNP

The (111) and (200) peaks of Pt:Pd catalysts were slightly shifted toward higher 2θ values, can be ascribed to an increase of Pd content with Pt:Pd catalyst [124]. The peaks of Pd metal in XRD patterns are not shown can be attributed to the limited amount of Pd presence or because it is amorphous [125].

The crystallite size of electro catalyst was obtained from XRD were using the (111) diffraction peaks according to the Debye-Scherrer equation [126]:

$$D = \frac{0.9\times\lambda}{B\times\cos\theta} \tag{14}$$

where D is the crystallite size (nm), $\boldsymbol{\lambda}$ is the wavelength of x-ray diffraction (0.154 nm), B is a full width at half maximum (FWHM) (radians), θ is the angle at the maximum of the peak (radians). A Gaussian procedure was used to determine the accuracy of peaks in order to find FWHM to calculate crystallites size. The crystallite size results are given in Table 4.2. A sample calculation for the determining of the crystallite size of catalysts is given in Appendix B.

The d-spacing (interplanar spacing between the atoms) of (111) planes for catalysts can be determined from XRD pattern from Bragg's law in the equation [127]:

$$d = \frac{n\times\lambda}{2\times\sin\theta} \tag{15}$$

where d is the distance between atomic layers in the crystal (Å), λ is X-ray wavelength (1.5406 Å), θ the angle of the peak, and n =1 is the order of reflection. The results for d-spacing were nearly the same, so the lattice constant for (111) diffraction peaks of Pt:Pd bimetallic was calculated from the below equation and the results shown in Table 4.2 [123].

$$\frac{1}{d^2} = \frac{h^2+k^2+l^2}{a^2} \tag{16}$$

where d is the distance between atomic layers in the crystal, hkl is miller indexes and a is lattice constant.

The determined lattice constants (a) show that the values of all catalysts between in the Pt (3.92 Å) and Pd (3.89 Å) that is, bimetallic catalysts have formed a solid structure together [128]. In addition, the results show that there are different ratios of

Pt and Pd loading to different support materials since each catalyst has a different constant.

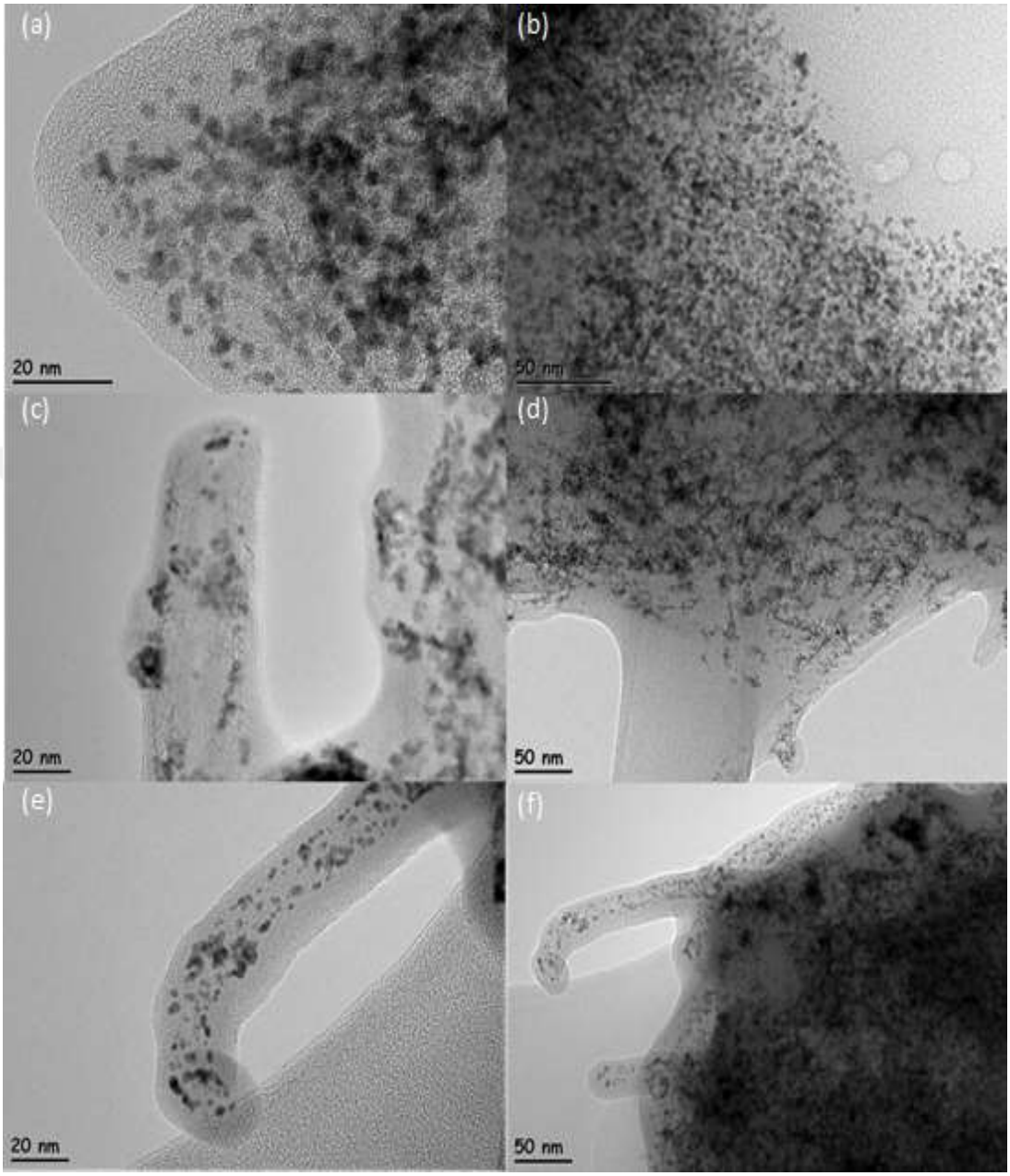

Figure 4.3. TEM images of a-b for Pt:Pd/GNP, c-d for Pt:Pd/MWCNT and e-f for Pt:Pd/MWCNT-GNP catalysts.

Distribution onto the support material is an important factor for enhancing the electrocatalytic activity and efficiency of the electrocatalyst [21]. The TEM images of Pt:Pd/GNP, Pt:Pd/MWCNT and Pt:Pd/MWCNT-GNP catalysts are shown in Figure 4.3. As shown in Figure 4.3 (a–f), it was observed that the particles were

uniformly distributed on supports. The particle size distribution percentage results for Pt:Pd/GNP, Pt:Pd/MWCNT, and Pt:Pd/MWCNT-GNP are shown in Figure 4.4. The TEM results show that the shape of the bimetallic catalyst nanoparticles is nearly spherical and the most particles correspond to the optimal sizes for improving HER kinetics, where superior size ranging from 2-4 nm [65]. The average particle size was found as 2.47 nm, 2.54 nm and 2.70 for Pt:Pd/GNP, Pt:Pd/MWCNT and Pt:Pd/MWCNT-GNP catalysts, respectively.

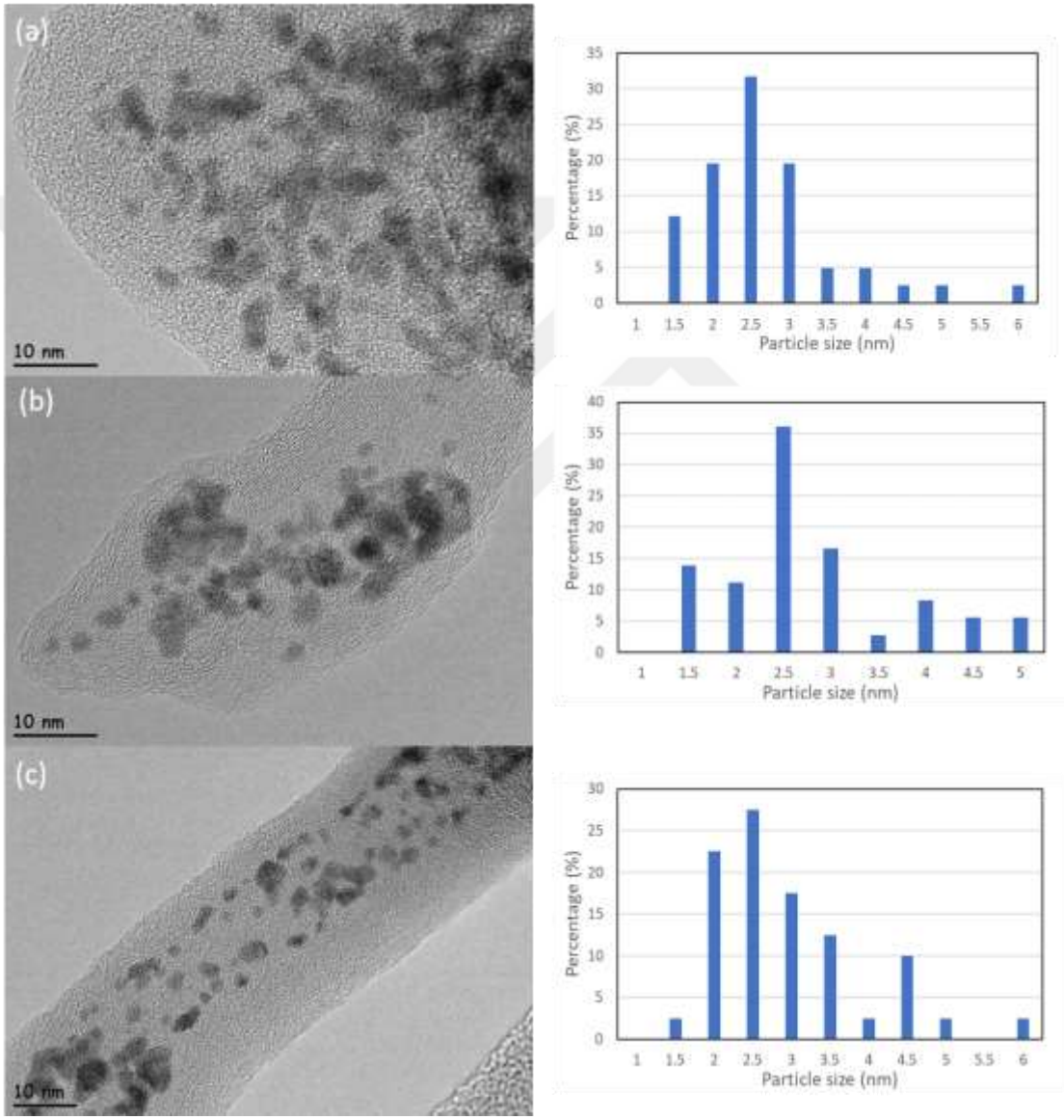

Figure 4.4. TEM images for particle size distribution of a) Pt:Pd/GNP, b) Pt:Pd/ MWCNT and c) Pt:Pd/ MWCNT-GNP catalysts

The Pt:Pd/MWCNT-GNP, have higher conductivity and higher performance of microwave absorption than the pure of GNP or pure of MWCNT, this is due to the fusion of defects and the ease of transmission of electrons as well as the increase of the basal divergence [129], [130]. As a result of using EG as a dispersant agent, it helps in a good distribution of nanoparticles, reduces particle agglomeration and improves stability [131]. As a result of the synergistic correlation between GNP and MWCNT, it prevents the accumulation of G layers and provides particle deposition at active sites. The crystal size distribution in MWCNT-GNP is smaller than the rest of the catalysts.

The mean particle sizes of the catalysts were calculated with Sauter mean diameter formula from TEM results [132] and the mean particle size results are given in Table 4.2 :

$$d_{32} = \frac{\sum_{i=1}^{n} n_i {d_i}^3}{\sum_{i=1}^{n} n_i {d_i}^2} \tag{17}$$

where n_i number of particles in size range i, d_i diameter of the particle in size range i which calculated from TEM analysis.

Table 4.2. Average crystallite size, mean particle size and lattice constant

Catalyst Name	Lattice constant ($\mathbf{A^0}$)	Average crystallite size by XRD (nm)	Mean Particle size by TEM (nm)
Pt:Pd/GNP	3.900	2.3	3.30
Pt:Pd/MWCNT	3.910	2.6	3.25
Pt:Pd/MWCNT-GNP	3.914	2.1	3.40

The Selected Area Electronic Diffraction (SAED) diagram corresponding to (111), (200), (220) and (311) planes of FCC structure and (002) plane of graphite observed high intensity diffraction rings for Pt:Pd/MWCNT-GNP catalyst among other catalysts given in Figure 4.5. According to SAED and differences between the average crystallite size and mean particle size, most Pt:Pd particles were well dispersed on the support material but a few agglomerations were observed.

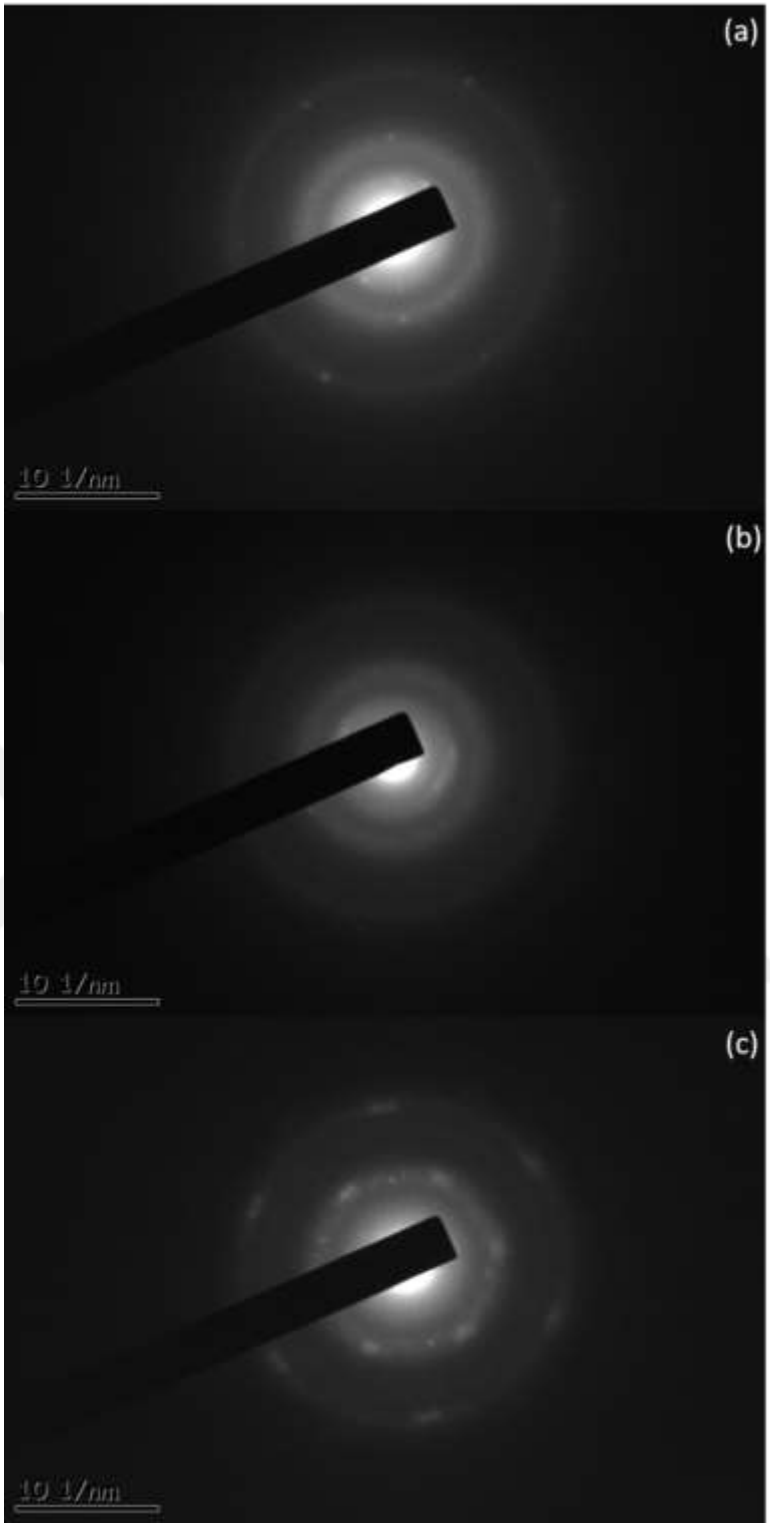

Figure 4.5. TEM images of (a) Pt:Pd/GNP, (b) Pt:Pd/MWCNT, and (c) Pt:Pd/MWCNT-GNP catalysts

4.2. Electrochemical Characterization

4.2.1. Cyclic voltammetry (CV) Results

The CV curves of catalysts given in Figure 4.6, illustrate three distinct regions: H_2 adsorption/desorption peaks region, a double layer region, and a metal oxidation/ reduction region. The electrochemical surface area shows the efficient Pt:Pd active sites for HER where triple-phase contact of catalyst, reactant gas, and the membrane happen to perform the electrochemical reaction leading to more effective use of metal particles [21].

The CV curves showed the cathodic peaks of the catalysts where Pt:Pd/MWCNT-GNP showed the highest current density peak of approximately -0.00055 A at about 0.33 V compared with the Pt:Pd/GNP was -0.00042 A at 0.36 V and Pt:Pd/MWCNT was -0.00038 A at 0.38 V. That indicates that the highest current density and the lowest overpotential of Pt:Pd/MWCNT-GNP even after 1000 cycles, which improves the activity of the catalyst. This confirms that Pt:Pd/MWCNT-GNP is the best catalyst compared to other catalysts in terms of activity, stability, and durability.

ECSA is determined by calculating the combined charge in the H_2 adsorption /desorption region after the correction of the double layer [133]. As a result of CV tests for the catalysts, ECSA was calculated according Tymen et. al.[134] :

$$\text{ECSA} = \frac{1}{(2.1\times10^{-4})}\frac{Q_H}{m_{(ptpd)}} \tag{18}$$

where $m_{(PtPd)}$ is the mass of PtPd on GC electrode, $2.1x10^{-4}$ is the charge constant value, and Q_H is the charge of H_2 adsorption/desorption [134].

All catalysts showed a marked decrease in the ECSA values. The ECSA losses of the catalysts which calculated from initial and final values of ECSA, given in Table 4.3 [135]. Although the initial ECSA for Pt:Pd/MWCNT-GNP is less than both Pt:Pd/GNP and Pt:Pd/MWCNT, the ECSA loss is lower than other catalysts that indicate it is more stable and long-term durability. The low value can be explained by the size of the particle.

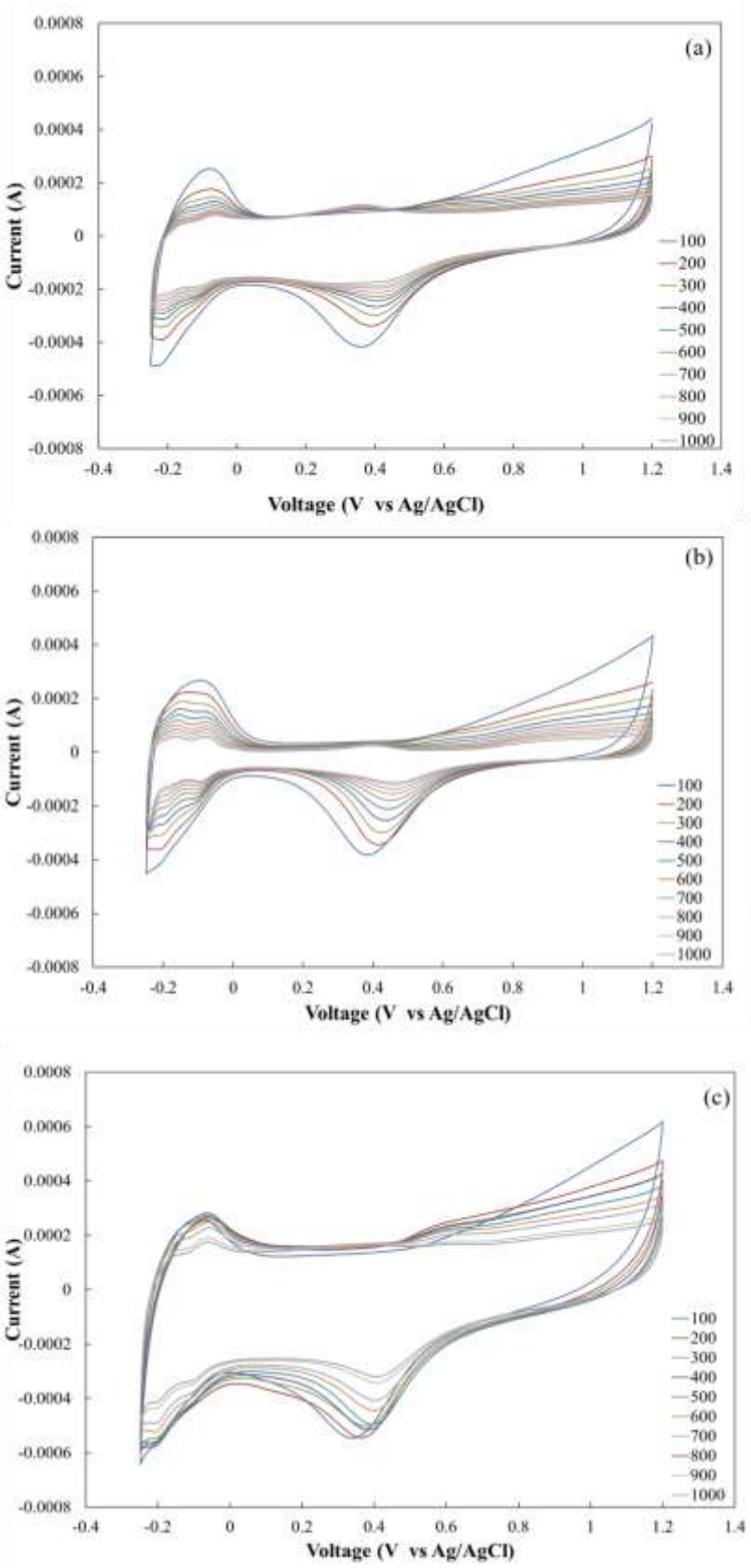

Figure 4.6. CV of the (a) Pt:Pd/GNP , (b) Pt:Pd/MWCNT and (c) Pt:Pd/MWCNT-GNP at room temperature in N_2 purged 0.1M $HClO_4$ solution for 1000 cycle

The specific surface area (SSA) of the bimetallic catalysts can be determined from the below equation [136]:

$$SSA = \frac{6000}{\rho_{PtPd} \times d} \quad (19)$$

where ρ is the PtPd density, d (nm) is the PtPd diameter which calculated from the XRD. The PtPd density was calculated as follows [137]:

$$\rho_{PtPd} = \rho_{Pt} x_{Pt} + \rho_{Pd} x_{Pd} \quad (20)$$

where ρ_{Pt} is the platinum density (21.4 g/cm^3), ρ_{Pd} is the palladium density (11.9 g/cm^3) and x_{Pt} and x_{Pd} are molar fractions of Pt and Rd in the bimetallic catalyst without support. Pt:Pd atomic ratio is 0.6:0.4, 0.52:0.48, 0.58:0.42 for PtPd/GNP, PtPd/MWCNT and PtPd/MWCNT-GNP catalysts, respectively.

As seen from Table 4.3, the highest SSA is examined for the catalyst Pt:Pd/MWCNT-GNP catalyst compared to other catalysts due to the smaller diameter. The reduced SSA related to increased diameter leads to performance losses in the catalyst and also causes to reduced homogeneity thus caused to loss of activity of the catalysts [22].

The Pt utilization efficiency of the catalysts is the ratio of the electrochemical surface area to the SSA of the catalysts was calculated from the following equation [138]:

$$U_{PtPd}(\%) = \frac{ECSA}{SSA} x100 \quad (21)$$

Table 4.3.ECSA and ECSA loss values of the catalysts

Catalyst	ECSA initial (m^2/g)	ECSA final (m^2/g)	ECSA loss (%)	SSA (m^2/g)	U_{PtPd} (%)
Pt:Pd/GNP	53.5	8.6	84	148	36
Pt:Pd/MWCNT	71.7	20.02	72	137	52
Pt:Pd/MWCNT-GNP	43.8	22.6	48	164	27

The utilization results showed that the highest utilization efficiency of Pt:Pd/MWCNT catalyst (52 %) while the lowest utilization efficiency of Pt:Pd/MWCNT-GNP catalyst (27 %). The high utilization shows a decrease in the contact area of the support material and Pt:Pd metals. Also high utilization efficiency reduces the correlation between catalyst and support while the lower utilization efficiency indicates better catalyst preference [13].

4.2.2. HT-PEMFC Test Results

The acid doping and acid leaching results of the prepared membranes were obtained as 13 and 85 %, respectively. The HT-PEMFC performance tests were conducted at 160°C and ambient pressure. HT-PEMFC performance tests were carried out at 160^{o}C. In the literature, HT-PEMFC studies are carried out between 140-180°C. In our previous studies, the best HT-PEMFC performance was achieved at 160°C [139]. High operating temperatures cause problems in performance tests due to the degradation of components such as gaskets and connections in the cell at temperatures above 160^{o}C.

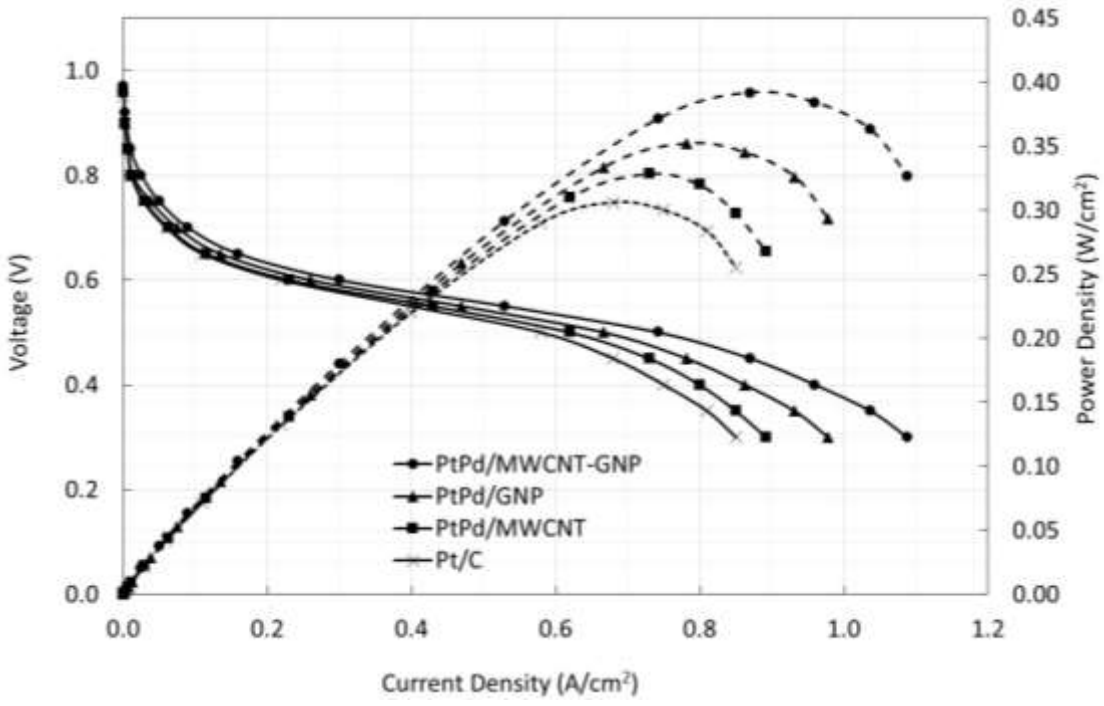

Figure 4.7. HT-PEMFC performance curves with H_2/air at 160°C.

The synthesized catalysts were evaluated, to study the effect of various carbon supports on catalyst performance. Figure 4.7 shows the polarization curves of HT-

PEMFC with Pt:Pd/MWCNT-GNP, Pt:Pd/MWCNT, Pt:Pd/GNP and Pt/C catalysts as feeding pure H_2/Air (supplied at 1.2 and 2.5 Stochiometric flow) at 160°C. The open-circuit voltages (OCV) were changed between 0.95–0.97 V. The OCV value of MWCNT-GNP indicates that the H_3PO_4 doped PBI membrane contains low H_2 crossover [27].

The results of the performance tests for different catalysts at 160°C in pure H_2/air shown in Table 4.4. When the prepared MEA were compared with the Pt:Pd/MWCNT-GNP, Pt:Pd/GNP, Pt:Pd/MWCNT and Pt/C catalysts, the current densities at 0.6V were 0.3, 0.26, 0.23, and 0.22 A/cm^2 ,respectively and the power densities received to 0.18, 0.156, 0.14, and 0.13 W/cm^2 ,respectively.

Table 4.4. Performance test results with H_2/air at 160°C

Catalyst	OCV	Power density at 0.6V (W/cm^2)	Current density at 0.6V (W/cm^2)	Max.power density (W/cm^2)
Pt:Pd/GNP	0.96	0.16	0.26	0.35
Pt:Pd/MWCNT	0.96	0.14	0.23	0.33
Pt:Pd/MWCNT-GNP	0.97	0.18	0.30	0.39
Pt/C	0.95	0.13	0.22	0.31

The maximum power densities of Pt:Pd/MWCNT-GNP, Pt:Pd/GNP, Pt:Pd/MWCNT and Pt/C were 0.39, 0.35, 0.33, 0.31 W/cm^2, respectively. The weakest performance was observed from the Pt/C catalyst this ascribed to the lower surface area and poor electrical conductivity compared to the rest of catalysts [140]. The HT-PEMFC performance of Pt:Pd/MWCNT-GNP based MEA shows the best performance compared with the rest of catalysts due to has better characteristics such as high conductivity, stability, and durability.

A comparison of the HT-PEMFC catalysts based MEA with reformate gas (H_2/CO_2/CO:75/22/3)/Air at 160°C is shown in Figure 4.8. Reformate gas mixture concentrations used as 75 vol. % H_2, 22 vol. % CO_2 and 3 vol. % CO, because the ratios are ideal gas mixture outlet of reformate unit based on the literature [27].

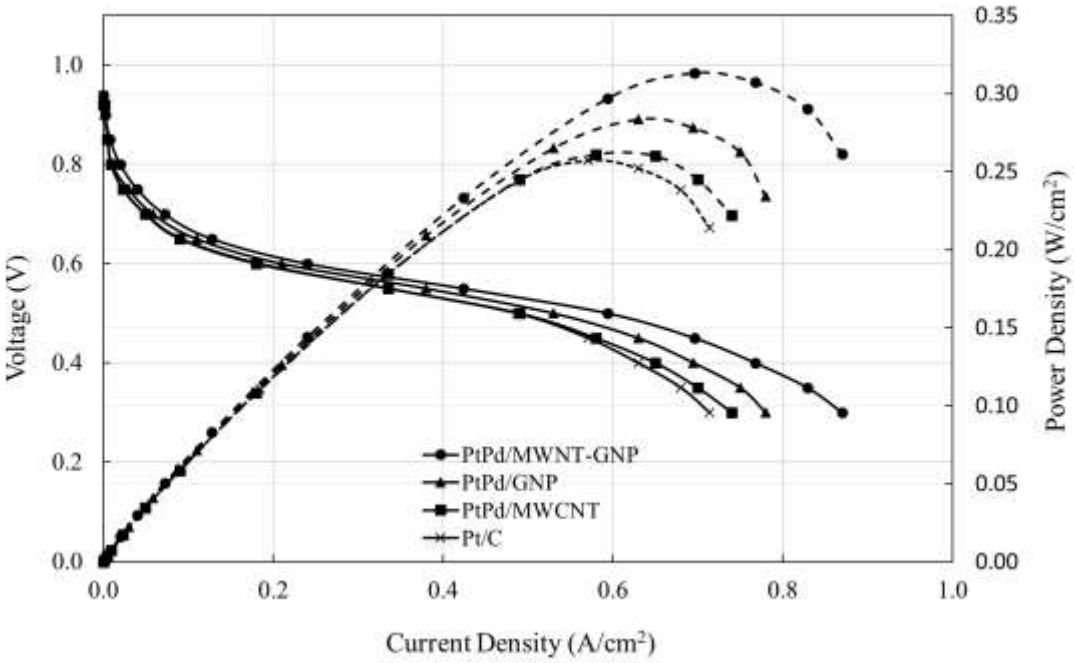

Figure 4.8. HT-PEMFC performance curves with reformate gas/air at 160°C.

The power densities and the current densities at 0.6 V of the Pt:Pd/MWCNT-GNP, Pt:Pd/GNP, Pt:Pd/MWCNT and Pt/C were 0.14, 0.126, 0.108, and 0.111 W/cm^2 and 0.240, 0.210, 0.180, and 0.185 A/cm^2 respectively. These results are shown in the Table 4.5. The maximum power densities of Pt:Pd/MWCNT-GNP, Pt:Pd/GNP, Pt:Pd/MWCNT and Pt/C were 0.31, 0.28, 0.26, 0.26 W/cm^2, respectively.

Table 4.5. Performance tests results with reformate gas/air at 160°C

Catalyst	OCV	Power density at 0.6V (W/cm^2)	Current density at 0.6V (W/cm^2)	Max.power density (W/cm^2)
Pt:Pd/GNP	0.94	0.126	0.210	0.28
Pt:Pd/MWCNT	0.92	0.108	0.180	0.26
Pt:Pd/MWCNT-GNP	0.94	0.140	0.240	0.31
Pt/C	0.94	0.111	0.185	0.26

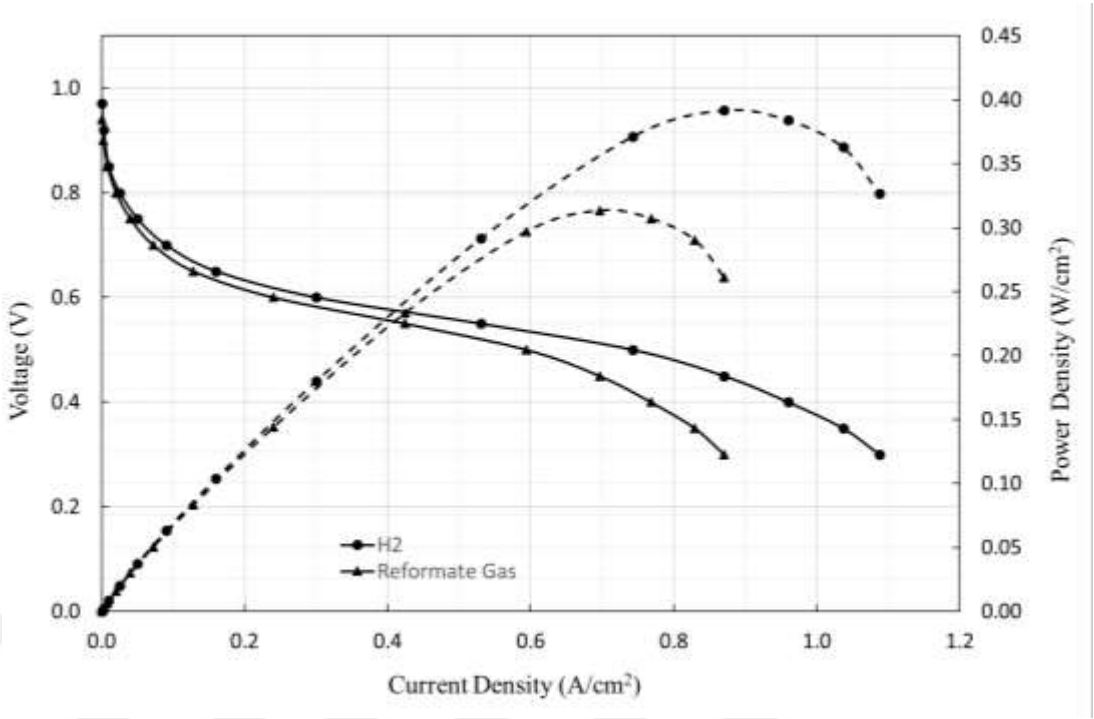

Figure 4.9. HT-PEMFC performance test for the Pt:Pd/MWCNT-GNP catalyst under reformate and H_2 gases at 160°C.

The HT-PEMFC performance curves of the Pt:Pd/MWCNT-GNP catalyst was compared for feeding of pure H_2/air and reformate gas/air at 160°C and ambient pressure are shown in Figure 4.9. According to the results, the Pt:Pd/MWCNT-GNP catalyst displayed the power density was 0.18 W/cm^2 and the current density was 0.3 A/cm^2 at 0.6 V in the H_2/air environment. But when using the reformate gas as a fuel instead of H_2 it is noted that the HT-PEMFC performance for Pt:Pd/MWCNT-GNP catalyst decreases where the power density was found to be 0.111 W/cm^2 while the current density was 0.240 A/cm^2 at 0.6 V for the same conditions. The reason for the decrease may be caused by the reverse water-gas exchange reaction (RWGS) ended up in the reduction of CO_2 into CO, caused by the high operating temperature. Since HT-PEMFC operates without humidification, electro-oxidation of CO is neglected. The moisture-free supply of the anode gas stream exchanges the balance of CO formation with the reverse water-gas exchange reaction ($H_2 + CO_2 \rightarrow H_2O + CO$) [27]. The water was constituted due to this reaction, may block the pores of the synthesis catalyst that used in MEA and caused loss of performance [141].

Based on the results of the HT-PEMFC performance test, the catalyst Pt:Pd/MWCNT-GNP shows the higher performance in both environments, so the catalyst is considered as a suitable catalyst for HT-PEMFC in both fuels. The reformate gas is used as a fuel to commercialize the operation of the HT-PEMFC because the remaining CO in the reformate gas is less absorbed on the Pt active site. Previous studies have shown that long-term durability testing with HT-PEMFC using reformate gas could be fundamental for future design [27].

CHAPTER 5

CONCLUSIONS

This study indicates the comparison of various supports used in order to disperse the Pt:Pd nanoparticles over MWCNT-GNP, MWCNT and GNP support via microwave assisted synthesis at 600 W, 60 s. The operating temperature of the PBI based HT-PEMFC was 160^{o}C. The activity of catalysts was determined by characterizing structural and electrochemical measurements. The results of the TGA test indicated that the Pt:Pd/MWCNT-GNP catalyst has better thermal stability than Pt:Pd/MWCNT or Pt:Pd/GNP alone. XRD analysis was used to estimate the crystallite size and crystallite structure of catalysts. The results of XRD analysis showed that the smaller crystallite size belonged to Pt:Pd/MWCNT-GNP catalyst (2.1 nm). The results of TEM analysis showed that prepared catalysts have a good distribution for nanoparticles and the mean particle sizes of catalysts were calculated. Even the MWCNT-GNP has the smallest crystallite size, it also has the maximum mean particular size.

CV measurements were used to determine the ECSA for the catalysts. CV results showed that Pt:Pd/MWCNT was the highest ECSA than the rest catalysts but also had the biggest ECSA loss. Although the initial ECSA of Pt:Pd/MWCNT-GNP is lower than both Pt:Pd/GNP and Pt:Pd/MWCNT, it showed higher ECSA after 1000 cycles and less ECSA loss that indicates its more stable and it has longer durability. According to CV calculation, the SSA and utilization efficiency of the catalysts were also calculated. The results showed that the highest SSA was determined for Pt:Pd /MWCNT-GNP catalyst as 164 m^2/g compared to the other catalysts. As a result, it can be concluded that Pt:Pd/MWCNT-GNP catalyst has enhanced electrocatalytic activity than Pt:Pd/MWCNT and Pt:Pd/GNP catalysts due to the synergistic interaction between Pt and Pd particles on MWCNT-GNP hybrid support.

HT-PEMFC performance test results showed that the best performance of the Pt:Pd/MWCNT-GNP catalyst compared to the rest of the catalysts. It was observed that the Pt:Pd/MWCNT-GNP catalyst showed higher performance with H_2 compared to the reformate gas environment.

It can be concluded that Pt:Pd/MWCNT-GNP bimetallic catalyst considers more suitable catalyst for HT-PEMFC due to it has high characteristics such as catalytic activity, improved HT-PEMFC performance, catalyst efficiency and improved long-term durability. The reasons of these advantages were related to bimetallic synergistic effect of the catalysts and the hybrid structure of MWCNT-GNP.

In order to develop the study, the following subjects can be emphasized in the following studies:

- Bimetallic catalysts can be prepared with different support material to be observed the different support material effects.
- Bimetallic catalysts can be synthesized with different molar ratios to observe the loading effect for Pt and Pd.
- HT-PEMFC stack can be prepared with Pt:Pd/MWCNT-GNP catalyst to observed stack performance.

REFERENCES

[1] F. Barbir, 'Front Matter', in PEM Fuel Cells, Elsevier, 2013.

[2] M. Liu, C. Zhang, and W. Chen, Novel Nanomaterials as Electrocatalysts for Fuel Cells. Elsevier Inc., 2018.

[3] S. Pasupathi, J. C. C. Gomez, H. Su, H. Reddy, P. Bujlo, and C. Sita, Recent Advances in High-Temperature PEM Fuel Cells. 2016.

[4] K. K. Karuppanan, M. K. Panthalingal, and P. Biji, Nanoscale, Catalyst Support Materials for Proton-Exchange Membrane Fuel Cells. Elsevier Inc., 2018.

[5] P. G. Technologies and P. Breeze, 'Fuel Cells', pp. 145–171, 2019.

[6] Y. Devrim and A. Albostan, 'Enhancement of PEM fuel cell performance at higher temperatures and lower humidities by high performance membrane electrode assembly based on Nafion/zeolite membrane', Int. J. Hydrogen Energy, vol. 40, no. 44, pp. 15328–15335, 2015.

[7] S. V. M. Guaitolini and J. F. Fardin, "Fuel Cells: History (Short Remind), Principles of Operation, Main Features, and Applications," in Advances in Renewable Energies and Power Technologies, vol. 2, Elsevier, 2018, pp. 123–150.

[8] H. Mohammed, S. Authayanun, P. Nancarrow, M. Tawalbeh, M. El, and H. Assad, 'Direct Hydrocarbon Fuel Cells : A Promising Technology for Improving', Energy, 2019.

[9] A. Coralli, B. J. M. Sarruf, P. E. V. de Miranda, Luigi Osmieri, S. Specchia, and N. Q. Minh, Chapter 2 - Fuel Cells. Elsevier Inc., 2019.

[10] S. Schlick, The chemistry of membranes used in fuel cells: Degradation and stabilization. 2018.

[11] A. Schenk, B. Cermenek, and V. Hacker, Other Polymer Electrolyte Fuel Cells. Elsevier Inc., 2018.

[12] A. Iwan, M. Malinowski, and G. Pasciak, 'Polymer fuel cell components

modified by graphene: Electrodes, electrolytes and bipolar plates', Renew. Sustain. Energy Rev., vol. 49, pp. 954–967, 2015.

[13] B. S. and G. Spazzafumo, Hydrogen and fuel cells: emerging technologies and applications. 2018.

[14] C. Gupta, P. H. Maheshwari, and S. R. Dhakate, 'Development of multiwalled carbon nanotubes platinum nanocomposite as efficient PEM fuel cell catalyst', Mater. Renew. Sustain. Energy, vol. 5, no. 1, pp. 1–11, 2016.

[15] Y. Nalbant, C. O. Colpan, and Y. Devrim, 'Energy and exergy performance assessments of a high temperature-proton exchange membrane fuel cell based integrated cogeneration system', Int. J. Hydrogen Energy, pp. 1–11, 2019.

[16] A. Kulikovsky, "Analytical modelling of fuel cells, Fuel cell basics," in Stationary Fuel Cells, Elsevier, 2019, pp. 1–33.

[17] S. Prakash, W. E. Mustain, and P. A. Kohl, Electrolytes for Long-Life, Ultra Low-Power Direct Methanol Fuel Cells. Elsevier Inc., 2009.

[18] S. Limpattayanate and M. Hunsom, 'ORR Activity and Stability of Pt-Based Electrocatalysts in PEM Fuel Cell', vol. 9, no. 5, pp. 647–657, 2015.

[19] W. Zhang, P. Sherrell, A. I. Minett, J. M. Razal, and J. Chen, 'Carbon nanotube architectures as catalyst supports for proton exchange membrane fuel cells', Energy Environ. Sci., vol. 3, no. 9, pp. 1286–1293, 2010.

[20] Y. Shao, G. Yin, Z. Wang, and Y. Gao, 'Proton exchange membrane fuel cell from low temperature to high temperature: Material challenges', J. Power Sources, vol. 167, no. 2, pp. 235–242, 2007.

[21] Y. Devrim, E. D. Arıca, and A. Albostan, 'Graphene based catalyst supports for high temperature PEM fuel cell application', Int. J. Hydrogen Energy, vol. 43, no. 26, pp. 11820–11829, 2018.

[22] E. S. Şayin, A. Bayrakçeken, and I. Eroğlu, 'Durability of PEM fuel cell electrocatalysts prepared by microwave irradiation technique', Int. J. Hydrogen Energy, vol. 37, no. 21, pp. 16663–16672, 2012.

[23] J. Wu et al., ‘A review of PEM fuel cell durability : Degradation mechanisms and mitigation strategies’, vol. 184, pp. 104–119, 2008.

[24] S. Authayanun, K. Im, and A. Arpornwichanop, ‘Review (Special Column on Electrocatalysis for Fuel Cells) A review of the development of high temperature proton exchange membrane fuel cells’, vol. 36, no. 4, pp. 473–483, 2015.

[25] F. Maillard, N. Job, and M. Chatenet, Basics of PEMFC Including the Use of Carbon-Supported Nanoparticles, Error. Elsevier B.V., 2013.

[26] S. Basu, ‘Proton exchange membrane fuel cell technology: India’s perspective’, Proc. Indian Natl. Sci. Acad., vol. 81, no. 4, pp. 865–890, 2015.

[27] Y. Devrim, A. Albostan, and H. Devrim, ‘Experimental investigation of CO tolerance in high temperature PEM fuel cells’, Int. J. Hydrogen Energy, vol. 43, no. 40, pp. 18672–18681, 2018.

[28] D. G. Caglayan, B. Sezgin, Y. Devrim, and I. Eroglu, ‘Three-dimensional modeling of a high temperature polymer electrolyte membrane fuel cell at different operation temperatures’, Int. J. Hydrogen Energy, vol. 41, no. 23, pp. 10060–10070, 2016.

[29] Y. Özdemir, N. Üregen, and Y. Devrim, ‘Polybenzimidazole based nanocomposite membranes with enhanced proton conductivity for high temperature PEM fuel cells’, Int. J. Hydrogen Energy, vol. 42, no. 4, 2017.

[30] P. Chippar and H. Ju, ‘Numerical modeling and investigation of gas crossover effects in high temperature proton exchange membrane (PEM) fuel cells’, Int. J. Hydrogen Energy, vol. 38, no. 18, pp. 7704–7714, 2013.

[31] R. E. Rosli et al., ‘A review of high-temperature proton exchange membrane fuel cell (HT-PEMFC) system’, Int. J. Hydrogen Energy, vol. 42, no. 14, pp. 9293–9314, 2017.

[32] S. S. Araya et al., ‘A comprehensive review of PBI-based high temperature PEM fuel cells’, Int. J. Hydrogen Energy, vol. 41, no. 46, pp. 21310–21344, 2016.

[33] S. Neophytides, M. K. Daletou, N. Athanasopoulos, N. Gourdoupi, E. De Castro, and M. Schautz, 'High Temperature PEM Fuel Cell Stacks with Advent TPS Meas', in E3S Web of Conferences 16, 2017, vol. 10002, no. 1, pp. 4–7.

[34] G. Umur, A. Yilser, and D. C. Ozgur, 'Performance of an HT - PEMFC having a catalyst with graphene and multiwalled carbon nanotube support', no. November 2018, pp. 1–12, 2019.

[35] V. K. Krastev, G. Falcucci, E. Jannelli, M. Minutillo, and R. Cozzolino, '3D CFD modeling and experimental characterization of HT PEM fuel cells at different anode gas compositions', Int. J. Hydrogen Energy, vol. 39, no. 36, pp. 21663–21672, 2014.

[36] M. A. Haque, A. B. Sulong, K. S. Loh, E. H. Majlan, T. Husaini, and R. E. Rosli, 'Acid doped polybenzimidazoles based membrane electrode assembly for high temperature proton exchange membrane fuel cell: A review', Int. J. Hydrogen Energy, vol. 42, no. 14, pp. 9156–9179, 2017.

[37] H. R. Ellamla, I. Staffell, P. Bujlo, B. G. Pollet, and S. Pasupathi, 'Current status of fuel cell based combined heat and power systems for residential sector', J. Power Sources, vol. 293, pp. 312–328, 2015.

[38] E. Jannelli, M. Minutillo, and A. Perna, 'Analyzing microcogeneration systems based on LT-PEMFC and HT-PEMFC by energy balances', Appl. Energy, vol. 108, pp. 82–91, 2013.

[39] Y. Garsany, B. D. Gould, O. A. Baturina, and K. E. Swider-Lyons, 'Comparison of the sulfur poisoning of PBI and Nafion PEMFC cathodes', Electrochem. Solid-State Lett., vol. 12, no. 9, pp. B138–B140, 2009.

[40] L. Barelli, G. Bidini, F. Gallorini, and A. Ottaviano, 'An energetic-exergetic analysis of a residential CHP system based on PEM fuel cell', Appl. Energy, vol. 88, no. 12, pp. 4334–4342, 2011.

[41] D. D. Boettner and M. J. Moran, 'Proton exchange membrane (PEM) fuel cell-powered vehicle performance using direct-hydrogen fueling and on-board methanol reforming', Energy, vol. 29, no. 12–15 SPEC. ISS., pp. 2317–2330,

2004.

[42] Q. Li, J. O. Jensen, R. F. Savinell, and N. J. Bjerrum, ‘High temperature proton exchange membranes based on polybenzimidazoles for fuel cells’, Prog. Polym. Sci., vol. 34, no. 5, pp. 449–477, 2009.

[43] H. Sun and H. C. Y. Wan, ‘Mass transfer in the HT-PEM fuel cell electrode’, Energy Procedia, vol. 61, pp. 1524–1527, 2014.

[44] S. H. Hsieh, M. C. Hsu, W. L. Liu, and W. J. Chen, ‘Study of Pt catalyst on graphene and its application to fuel cell’, Appl. Surf. Sci., vol. 277, pp. 223–230, 2013.

[45] H. Cruz-Martínez et al., ‘Mexican contributions for the improvement of electrocatalytic properties for the oxygen reduction reaction in PEM fuel cells’, Int. J. Hydrogen Energy, pp. 12477–12491, 2019.

[46] N. Üregen, K. Pehlivanoğlu, Y. Özdemir, and Y. Devrim, ‘Development of polybenzimidazole/graphene oxide composite membranes for high temperature PEM fuel cells’, Int. J. Hydrogen Energy, vol. 42, no. 4, pp. 2636–2647, 2017.

[47] K. Takeuchi et al., ‘Hydrogen Permeation in Hydrated Perfluorosulfonic Acid Polymer Membranes: Effect of Polymer Crystallinity and Equivalent Weight’, J. Phys. Chem. C, vol. 123, no. 33, pp. 20628–20638, 2019.

[48] Y. Devrim, H. Devrim, and I. Eroglu, ‘Polybenzimidazole/SiO2 hybrid membranes for high temperature proton exchange membrane fuel cells’, Int. J. Hydrogen Energy, vol. 41, no. 23, pp. 10044–10052, 2016.

[49] Y. Özdemir, N. Üregen, and Y. Devrim, ‘Polybenzimidazole based nanocomposite membranes with enhanced proton conductivity for high temperature PEM fuel cells’, Int. J. Hydrogen Energy, vol. 42, no. 4, pp. 2648–2657, 2017.

[50] W. Kimberley, Fuel cells, vol. 29, no. 2. 2004.

[51] R. P. Singh, G. J. Dahe, K. W. Dudeck, C. F. Welch, and K. A. Berchtold, ‘High temperature polybenzimidazole hollow fiber membranes for hydrogen

separation and carbon dioxide capture from synthesis gas', Energy Procedia, vol. 63, pp. 153–159, 2014.

[52] J. O. Jensen, D. Aili, Y. Hu, L. N. Cleemann, and Q. Li, High-Temperature Polymer Electrolyte Membrane Fuel Cells. Springer International Publishing, 2019.

[53] L. N. Cleemann et al., 'Catalyst degradation in high temperature proton exchange membrane fuel cells based on acid doped polybenzimidazole membranes', Fuel Cells, vol. 13, no. 5, pp. 822–831, 2013.

[54] J. L. Jespersen, E. Schaltz, and S. K. Kær, 'Electrochemical characterization of a polybenzimidazole-based high temperature proton exchange membrane unit cell', J. Power Sources, vol. 191, no. 2, pp. 289–296, 2009.

[55] R. Zeis, 'Materials and characterization techniques for high-temperature polymer electrolyte membrane fuel cells', Beilstein J. Nanotechnol., vol. 6, no. 1, pp. 68–83, 2015.

[56] L. Du, Y. Shao, J. Sun, G. Yin, J. Liu, and Y. Wang, 'Advanced catalyst supports for PEM fuel cell cathodes', Nano Energy, vol. 29, pp. 314–322, 2016.

[57] E. H. Majlan, D. Rohendi, W. R. W. Daud, T. Husaini, and M. A. Haque, 'Electrode for proton exchange membrane fuel cells: A review', Renew. Sustain. Energy Rev., vol. 89, no. June 2017, pp. 117–134, 2018.

[58] I. Tubert-Brohman, W. Sherman, M. Repasky, and T. Beuming, 'Improved docking of polypeptides with glide', J. Chem. Inf. Model., vol. 53, no. 7, pp. 1689–1699, 2013.

[59] K. H. Fahim and E. A. MAlfayydh Hayder Dhahad, 'Effect of Geometric Design of the Flow Fields Plat on the Performance of A PEM Fuel Cell: A Review', Int. J. Sci. Eng. Res., vol. 8, no. 7, 2017.

[60] J. Zhang et al., 'High temperature PEM fuel cells', vol. 160, pp. 872–891, 2006.

[61] C. Nah et al., 'Effects of curing systems on the mechanical and chemical

ageing resistance properties of gasket compounds based on ethylene-propylene-diene-termonomer rubber in a simulated fuel cell environment', Int. J. Hydrogen Energy, vol. 40, no. 33, pp. 10627–10635, 2015.

[62] D. Fowler, V. Gurau, and D. Cox, 'Bridging the gap between automated manufacturing of fuel cell components and robotic assembly of fuel cell stacks', Energies, vol. 12, no. 19, pp. 2–15, 2019.

[63] A. C. Bhosale, M. A. Mahajan, and P. C. Ghosh, 'Optimization of contact resistance with better gasketing for a unitized regenerative fuel cell', Int. J. Hydrogen Energy, pp. 20953–20962, 2019.

[64] D. Lee, J. W. Lim, S. Nam, I. Choi, and D. G. Lee, 'Gasket-integrated carbon/silicone elastomer composite bipolar plate for high-temperature PEMFC', Compos. Struct., vol. 128, pp. 284–290, 2015.

[65] Y. Devrim and E. D. Arıca, 'Multi-walled carbon nanotubes decorated by platinum catalyst for high temperature PEM fuel cell', Int. J. Hydrogen Energy, vol. 44, no. 34, pp. 18951–18966, 2019.

[66] P. Lin, P. Zhou, and C. W. Wu, 'Multi-objective topology optimization of end plates of proton exchange membrane fuel cell stacks', J. Power Sources, vol. 196, no. 3, pp. 1222–1228, 2011.

[67] N. Ul Hassan, M. Kilic, E. Okumus, B. Tunaboylu, and A. M. Soydan, 'Experimental determination of optimal clamping torque for AB-PEM fuel cell', J. Electrochem. Sci. Eng., vol. 6, no. 1, p. 9, 2016.

[68] Y. H. Yu, J. W. Lim, and D. G. Lee, 'Composite sandwich endplates with a compliant pressure distributor for a PEM fuel cell', Compos. Struct., vol. 119, pp. 505–512, 2015.

[69] T. Dey, J. Deshpande, D. Singdeo, and P. C. Ghosh, 'Study of PEM Fuel Cell End Plate Design by Structural Analysis Based on Contact Pressure', J. Energy, vol. 2019, pp. 1–11, 2019.

[70] Y. Lin, J. A. McCarthy, K. R. Poeppelmeier, and L. D. Marks, Applications of Electron Microscopy in Heterogeneous Catalysis. Elsevier Inc., 2015.

[71] T. Sheng, Y. X. Jiang, N. Tian, Z. Y. Zhou, and S. G. Sun, Nanocrystal Catalysts of High-Energy Surface and Activity, 1st ed., vol. 177. Elsevier B.V., 2017.

[72] S. Sharma and B. G. Pollet, 'Support materials for PEMFC and DMFC electrocatalysts - A review', J. Power Sources, vol. 208, pp. 96–119, 2012.

[73] E. J. Oh, R. Hempelmann, V. Nica, I. Radev, and H. Natter, 'New catalyst supports prepared by surface modification of graphene- and carbon nanotube structures with nitrogen containing carbon coatings', J. Power Sources, vol. 341, pp. 240–249, 2017.

[74] Y. Lu, S. Du, and R. Steinberger-Wilckens, 'Three-dimensional catalyst electrodes based on PtPd nanodendrites for oxygen reduction reaction in PEFC applications', Appl. Catal. B Environ., vol. 187, pp. 108–114, 2016.

[75] S. M. M. Ehteshami and S. H. Chan, 'A review of electrocatalysts with enhanced CO tolerance and stability for polymer electrolyte membarane fuel cells', Electrochim. Acta, vol. 93, pp. 334–345, 2013.

[76] A. Bharti and G. Cheruvally, 'Surfactant assisted synthesis of Pt-Pd/MWCNT and evaluation as cathode catalyst for proton exchange membrane fuel cell', Int. J. Hydrogen Energy, vol. 43, no. 31, pp. 14729–14741, 2018.

[77] L. T. Soo, K. S. Loh, A. B. Mohamad, W. R. W. Daud, and W. Y. Wong, 'An overview of the electrochemical performance of modified graphene used as an electrocatalyst and as a catalyst support in fuel cells', Appl. Catal. A Gen., vol. 497, pp. 198–210, 2015.

[78] A. K. Singh, Structure, Synthesis, and Application of Nanoparticles. 2016.

[79] C. Luo, H. Xie, Q. Wang, G. Luo, and C. Liu, 'A review of the application and performance of carbon nanotubes in fuel cells', J. Nanomater., vol. 2015, 2015.

[80] S. X. Xiao, C. S. Huang, and Y. L. Li, Carbon Materials. 2017.

[81] N. Shaari and S. K. Kamarudin, 'Graphene in electrocatalyst and proton conductiong membrane in fuel cell applications: An overview', Renew.

Sustain. Energy Rev., vol. 69, no. May 2016, pp. 862–870, 2017.

[82] E. Daş, S. Alkan Gürsel, L. Işıkel Şanlı, and A. Bayrakçeken Yurtcan, 'Thermodynamically controlled Pt deposition over graphene nanoplatelets: Effect of Pt loading on PEM fuel cell performance', Int. J. Hydrogen Energy, vol. 42, no. 30, pp. 19246–19256, 2017.

[83] Q. Wan et al., 'Graphene nanoplatelets supported metal nanoparticles for electrochemical oxidation of hydrazine', Electrochem. commun., vol. 29, pp. 29–32, 2013.

[84] T. Maiyalagan, X. Wang, and A. Manthiram, 'Highly active Pd and Pd-Au nanoparticles supported on functionalized graphene nanoplatelets for enhanced formic acid oxidation', RSC Adv., vol. 4, no. 8, pp. 4028–4033, 2014.

[85] M. Rashad, F. Pan, A. Tang, M. Asif, and M. Aamir, 'Synergetic effect of graphene nanoplatelets (GNPs) and multi-walled carbon nanotube (MW-CNTs) on mechanical properties of pure magnesium', J. Alloys Compd., vol. 603, pp. 111–118, 2014.

[86] H. Zhang et al., 'Synergistic effect of carbon nanotube and graphene nanoplates on the mechanical, electrical and electromagnetic interference shielding properties of polymer composites and polymer composite foams', Chem. Eng. J., vol. 353, no. May, pp. 381–393, 2018.

[87] O. S. Asiq Rahman, M. Sribalaji, B. Mukherjee, T. Laha, and A. K. Keshri, 'Synergistic effect of hybrid carbon nanotube and graphene nanoplatelets reinforcement on processing, microstructure, interfacial stress and mechanical properties of Al2O3 nanocomposites', Ceram. Int., vol. 44, no. 2, pp. 2109–2122, 2018.

[88] A. A. Fedotov, S. A. Grigoriev, P. Millet, and V. N. Fateev, 'Plasma-assisted Pt and Pt-Pd nano-particles deposition on carbon carriers for application in PEM electrochemical cells', Int. J. Hydrogen Energy, vol. 38, no. 20, pp. 8568–8574, 2013.

[89] R. M. Félix-Navarro et al., 'Pt-Pd bimetallic nanoparticles on MWCNTs:

Catalyst for hydrogen peroxide electrosynthesis', J. Nanoparticle Res., vol. 15, no. 8, 2013.

[90] H. R. Cho and J. R. Regalbuto, 'The rational synthesis of Pt-Pd bimetallic catalysts by electrostatic adsorption', Catal. Today, vol. 246, pp. 143–153, 2015.

[91] X. Zhang, G. Wu, Z. Cai, and X. Chen, 'Dual-functional Pt-on-Pd supported on reduced graphene oxide hybrids: Peroxidase-mimic activity and an enhanced electrocatalytic oxidation characteristic', Talanta, vol. 134, pp. 132–135, 2015.

[92] S. S. Li et al., 'Branched platinum-on-palladium bimetallic heteronanostructures supported on reduced graphene oxide for highly efficient oxygen reduction reaction', J. Power Sources, vol. 272, pp. 1078–1085, 2014.

[93] J. H. Park, Y. Sohn, D. H. Jung, P. Kim, and J. B. Joo, 'Pt deposited Pt-Pd/C electrocatalysts with the enhanced oxygen reduction activity', J. Ind. Eng. Chem., vol. 36, pp. 109–115, 2016.

[94] D. Bogdal, Microwave-Assisted Polymerization, vol. 4. Elsevier B.V., 2012.

[95] A. K. Rathi, M. B. Gawande, R. Zboril, and R. S. Varma, 'Microwave-assisted synthesis - Catalytic applications in aqueous media', Coord. Chem. Rev., vol. 291, pp. 68–94, 2015.

[96] K. Kumar Patel and R. Purohit, 'Improved shape memory and mechanical properties of microwave-induced thermoplastic polyurethane/graphene nanoplatelets composites', Sensors Actuators, A Phys., vol. 285, pp. 17–24, 2019.

[97] T. D. Thanh, J. Balamurugan, N. H. Kim, and J. H. Lee, Recent Advances in Metal Alloy-Graphene Hybrids for Biosensors. Elsevier Inc., 2018.

[98] T. Athar, Smart precursors for smart nanoparticles, Second Edi. Elsevier Inc., 2014.

[99] S. Editor and A. Hubbard, Interface Science and Technology, vol. 1, no. C. 2004.

[100] K. S. S. Jensen, H. Sun, R. M. L. Werchmeister, K. Mølhave, and J. Zhang, 'Microwave synthesis of metal nanocatalysts for the electrochemical oxidation of small biomolecules', Curr. Opin. Electrochem., vol. 4, no. 1, pp. 124–132, 2017.

[101] H. El-Deeb and M. Bron, 'Microwave-assisted polyol synthesis of PtCu/carbon nanotube catalysts for electrocatalytic oxygen reduction', J. Power Sources, vol. 275, pp. 893–900, 2015.

[102] M. V. Martínez-Huerta and M. J. Lázaro, Electrocatalysts for low temperature fuel cells, vol. 285. 2017.

[103] J. R. Zapata-Fernández et al., 'Ultrasonic-assisted galvanic displacement synthesis of Pt–Pd/MWCNT for enhanced oxygen reduction reaction: Effect of Pt concentration', Int. J. Hydrogen Energy, vol. 42, no. 15, pp. 9806–9815, 2017.

[104] X. Zhong et al., 'PtPd alloy embedded in nitrogen-rich graphene nanopores: High-performance bifunctional electrocatalysts for hydrogen evolution and oxygen reduction', Carbon N. Y., vol. 114, pp. 740–748, 2017.

[105] K. Fu et al., 'Facile morphology controllable synthesis of PtPd nanorods on graphene-multiwalled carbon nanotube hybrid support as efficient electrocatalysts for oxygen reduction reaction', Mater. Res. Bull., vol. 108, pp. 187–194, 2018.

[106] S. Limpattayanate and M. Hunsom, 'Electrocatalytic activity of Pt-Pd electrocatalysts for the oxygen reduction reaction in proton exchange membrane fuel cells: Effect of supports', Renew. Energy, vol. 63, pp. 205–211, 2014.

[107] A. T. N. Nguyen and J. H. Shim, 'Seedless, one-step synthesis of porous Pt-Pd nanoflowers for electroreduction of oxygen in acidic medium', Appl. Surf. Sci., vol. 458, no. July, pp. 910–916, 2018.

[108] X. Xiong, W. Chen, W. Wang, J. Li, and S. Chen, 'Pt-Pd nanodendrites as oxygen reduction catalyst in polymer-electrolyte-membrane fuel cell', Int. J. Hydrogen Energy, vol. 42, no. 40, pp. 25234–25243, 2017.

[109] E. Daş, S. Alkan Gürsel, L. Işikel Şanli, and A. Bayrakçeken Yurtcan, ‘Comparison of two different catalyst preparation methods for graphene nanoplatelets supported platinum catalysts’, Int. J. Hydrogen Energy, vol. 41, no. 23, pp. 9755–9761, 2016.

[110] R. Imran Jafri, N. Rajalakshmi, and S. Ramaprabhu, ‘Nitrogen doped graphene nanoplatelets as catalyst support for oxygen reduction reaction in proton exchange membrane fuel cell’, J. Mater. Chem., vol. 20, no. 34, pp. 7114–7117, 2010.

[111] S. U. B. Ramakrishna, D. Srinivasulu Reddy, S. Shiva Kumar, and V. Himabindu, ‘Nitrogen doped CNTs supported Palladium electrocatalyst for hydrogen evolution reaction in PEM water electrolyser’, Int. J. Hydrogen Energy, vol. 41, no. 45, pp. 20447–20454, 2016.

[112] Y. Devrim and A. Albostan, ‘Graphene-Supported Platinum Catalyst-Based Membrane Electrode Assembly for PEM Fuel Cell’, J. Electron. Mater., vol. 45, no. 8, pp. 3900–3907, 2016.

[113] A. Bharti, G. Cheruvally, and S. Muliankeezhu, ‘Microwave assisted, facile synthesis of Pt/CNT catalyst for proton exchange membrane fuel cell application’, Int. J. Hydrogen Energy, vol. 42, no. 16, pp. 11622–11631, 2017.

[114] J. Moreira, P. Del Angel, A. L. Ocampo, P. J. Sebastián, J. A. Montoya, and R. H. Castellanos, ‘Synthesis, characterization and application of a Pd/Vulcan and Pd/C catalyst in a PEM fuel cell’, Int. J. Hydrogen Energy, vol. 29, no. 9, pp. 915–920, 2004.

[115] H. Erikson, M. Liik, A. Sarapuu, J. Kozlova, V. Sammelselg, and K. Tammeveski, ‘Oxygen reduction on electrodeposited Pd coatings on glassy carbon’, Electrochim. Acta, vol. 88, pp. 513–518, 2013.

[116] N. Üregen, K. Pehlivanoğlu, Y. Özdemir, and Y. Devrim, ‘Development of polybenzimidazole/graphene oxide composite membranes for high temperature {PEM} fuel cells’, Int. J. Hydrogen Energy, 2016.

[117] Y. Özdemir, N. Özkan, and Y. Devrim, ‘Fabrication and characterization of

cross-linked polybenzimidazole based membranes for high temperature PEM fuel cells', Electrochim. Acta, vol. 245, pp. 1–13, 2017.

[118] J. Shen, B. Yan, M. Shi, H. Ma, N. Li, and M. Ye, 'Fast and facile preparation of reduced graphene oxide supported Pt-Co electrocatalyst for methanol oxidation', Mater. Res. Bull., vol. 47, no. 6, pp. 1486–1493, 2012.

[119] Y. Devrim and E. D. Arıca, 'Investigation of the effect of graphitized carbon nanotube catalyst support for high temperature PEM fuel cells', Int. J. Hydrogen Energy, no. xxxx, pp. 1–9, 2019.

[120] D. J. Douglas and J. B. French, 'An improved interface for inductively coupled plasma-mass', Spectrochim. Acta Part B At. Spectrosc., vol. v.41B, n.3, no. 1986, pp. 197–204, 1986.

[121] F. Yang, Y. Zhang, P. F. Liu, Y. Cui, X. R. Ge, and Q. S. Jing, 'Pd-Cu alloy with hierarchical network structure as enhanced electrocatalysts for formic acid oxidation', Int. J. Hydrogen Energy, vol. 41, no. 16, pp. 6773–6780, 2016.

[122] Y. Devrim, S. Erkan, N. Baş, and I. Eroglu, 'Improvement of PEMFC performance with Nafion/inorganic nanocomposite membrane electrode assembly prepared by ultrasonic coating technique', Int. J. Hydrogen Energy, vol. 37, no. 21, pp. 16748–16758, 2012.

[123] L. Li and Y. Xing, 'Pt-Ru nanoparticles supported on carbon nanotubes as methanol fuel cell catalysts', AIChE Annu. Meet. Conf. Proc., pp. 2803–2808, 2006.

[124] V. A. Online, 'Uniform Pd – Pt alloy nanoparticles supported on graphite nanoplatelets with high electrocatalytic activity towards methanol oxidation †', 2015.

[125] S. Thanasilp, 'Effect of Pt : Pd atomic ratio in Pt e Pd / C electrocatalyst-coated membrane on the electrocatalytic activity of ORR in PEM fuel cells', Renew. Energy, vol. 36, no. 6, pp. 1795–1801, 2011.

[126] X. Chen, Z. Cai, and M. Oyama, 'Green synthesis of graphene – PtPd alloy

nanoparticles with high electrocatalytic performance for ethanol oxidation †', pp. 315–320, 2014.

[127] S. A. Al-Thabaiti, Z. Khan, and M. A. Malik, 'Bimetallic Ag-Ni nanoparticles as an effective catalyst for hydrogen generation from hydrolysis of sodium borohydride', Int. J. Hydrogen Energy, vol. 44, no. 31, pp. 16452–16466, 2019.

[128] K. Hermann, 'Parameter Tables of Crystals', in Crystallography and Surface Structure: An Introduction for Surface Scientists and Nanoscientists., Wiley-VCH, 2011, p. Appendix.

[129] Y. Chen, A. Zhang, L. Ding, Y. Liu, and H. Lu, 'AC', Compos. Part B, 2016.

[130] X. Zhou, J. Qiao, L. Yang, and J. Zhang, 'REVIEW A Review of Graphene-Based Nanostructural Materials for Both Catalyst Supports and Metal-Free Catalysts in PEM Fuel Cell Oxygen Reduction Reactions', pp. 1–25, 2014.

[131] R. Kiyani, S. Rowshanzamir, and M. Javad, 'Nitrogen doped graphene supported palladium-cobalt as a promising catalyst for methanol oxidation reaction : Synthesis, characterization and electrocatalytic performance', Energy, vol. 113, pp. 1162–1173, 2016.

[132] P. B. Kowalczuk and J. Drzymala, 'Physical meaning of the Sauter mean diameter of spherical particulate matter', Part. Sci. Technol., vol. 34, no. 6, pp. 645–647, 2016.

[133] Z. Cai, C. Liu, G. Wu, X. Chen, and X. Chen, 'Electrochimica Acta Green synthesis of Pt-on-Pd bimetallic nanodendrites on graphene via in situ reduction , and their enhanced electrocatalytic activity for methanol oxidation', Electrochim. Acta, vol. 127, pp. 377–383, 2014.

[134] S. Tymen, A. Undisz, M. Rettenmayr, and A. Ignaszak, 'Pt–Pd catalytic nanoflowers: Synthesis, characterization, and the activity toward electrochemical oxygen reduction', J. Mater. Res., vol. 30, no. 15, pp. 2327–2339, 2015.

[135] L. I. Şanli, V. Bayram, B. Yarar, S. Ghobadi, and S. A. Gürsel, 'Development of graphene supported platinum nanoparticles for polymer electrolyte

membrane fuel cells: Effect of support type and impregnation-reduction methods', Int. J. Hydrogen Energy, vol. 41, no. 5, pp. 3414–3427, 2016.

[136] Y. Garsany, I. L. Singer, and K. E. Swider-lyons, 'Impact of film drying procedures on RDE characterization of Pt / VC electrocatalysts', J. Electroanal. Chem., vol. 662, no. 2, pp. 396–406, 2011.

[137] T. Vidaković, M. Christov, and K. Sundmacher, 'A method for rough estimation of the catalyst surface area in a fuel cell', J. Appl. Electrochem., 2009.

[138] S. L. Knupp, W. Li, O. Paschos, T. M. Murray, J. Snyder, and P. Haldar, 'The effect of experimental parameters on the synthesis of carbon nanotube / nanofiber supported platinum by polyol processing techniques', vol. 6, pp. 0–8, 2008.

[139] Y. Budak and Y. Devrim, 'Investigation of micro-combined heat and power application of PEM fuel cell systems', Energy Convers. Manag., vol. 160, 2018.

[140] W. Zhang, J. Chen, G. F. Swiegers, Z. F. Ma, and G. G. Wallace, 'Microwave-assisted synthesis of Pt/CNT nanocomposite electrocatalysts for PEM fuel cells', Nanoscale, vol. 2, no. 2, pp. 282–286, 2010.

[141] M. Boaventura, I. Alves, P. Ribeirinha, and A. Mendes, 'The influence of impurities in high temperature polymer electrolyte membrane fuel cells performance', *Int. J. Hydrogen Energy*, vol. 41, no. 43, pp. 19771–19780, 2016.

APPENDIX A

A.1. PBI MEMBRANE ACID DOPING LEVEL AND ACID LOSS PERCENTAGE

Acid doping levels of the membrane is determined due to the following equation:

$$\text{Acid Doping Level} = \frac{W_{H3PO4}}{W_{dry}} \times \frac{\text{MWofPBIRepeatUnit}}{\text{MWof}H_3PO_4} \quad (22)$$

where W_{H3PO4} is the final weight of membrane after H_3PO_4 immersed process, W_{dry} is the dry weight of membrane before H_3PO_4 immersed process. The acid loss percentage calculated due to the given equation [46]:

$$\text{Acid Loss Percentage} = \frac{W_o - W_i}{W_a} \quad (23)$$

where W_0 is the weight after acid doping membrane, Wa is the weight of H_3PO_4 present in the membrane and Wi is the weight of the membrane after leaching.

APPENDIX B

B.1. SAMPLE CALCULATION OF CRYSTALLITES SIZE

The crystallite sizes of the metals were calculated according to the equation 14 :

$$d = \frac{0.9*\lambda}{B*cos\theta} \quad (14)$$

The values of FWHM (B) were determined by OriginPro software. The FWHM values are given in Table 0.1.

Table 0.1. Crystallites size calculation parameters

Catalysts	**2θ Rad**	**FWHM rad**	**Crystallite size nm**
Pt:Pd/GNP	0.349	0.065	2.27
Pt:Pd/MWCNT	0.349	0.057	2.60
Pt:Pd/MWCNT-GNP	0.349	0.070	2.10